

Review

A Review—Effect of Accelerating Methods on Gas Nitriding: Accelerating Mechanism, Nitriding Behavior, and Techno-Economic Analysis

Yu-Long Zhou ^{1,2,†}, Fan Xia ^{1,3,†}, Ai-Jun Xie ⁴ , Hao-Ping Peng ^{1,3}, Jian-Hua Wang ^{1,*}  and Zhi-Wei Li ^{1,3,4,*} 

¹ School of Materials Science and Engineering, Changzhou University, Changzhou 213164, China; zyl512803@163.com (Y.-L.Z.); xf199901200120@163.com (F.X.); php@cczu.edu.cn (H.-P.P.)

² Jiangsu Institute, China Academy of Machinery Science & Technology Co., Ltd., Changzhou 213100, China

³ School of Petroleum and Natural Gas Engineering, Changzhou University, Changzhou 213164, China

⁴ Chemical and Biomolecular Engineering, National University of Singapore, Singapore 119077, Singapore; axie26@wisc.edu

* Correspondence: wangjh@cczu.edu.cn (J.-H.W.); lzw@cczu.edu.cn (Z.-W.L.)

† These authors contributed equally to this work.

Abstract: Gas nitriding, as a surface modification technology to improve the wear resistance of work-piece surfaces, is widely used in wind turbine gears, pressure vessel gears, high-precision die casting abrasives, and other areas. However, the gas nitriding time is too long, reaching 40–60 h, which reduces the efficiency of nitriding and hinders the development of gas nitriding. Therefore, various accelerating methods are born accordingly. This review first introduces the basic principle, microstructure, and process parameters of conventional gas nitriding. Then, five common accelerating methods are summarized: process parameter optimization, surface mechanical nano-crystallization, surface-active catalysis, surface pre-oxidation, and surface laser treatment. Then, the effect of acceleration methods on gas nitriding is analyzed for the acceleration mechanism, nitriding behavior, and nitriding efficiency. Finally, the technical economy of the acceleration methods is compared for three aspects: energy consumption, carbon dioxide emission, and cost. And, the technical maturity of the acceleration methods is compared according to technology readiness level (TRL) technology. Based on the above content, the advantages and disadvantages of the five accelerating methods are reviewed, and the concept of a multi-technology collaborative processing acceleration method is proposed.

Keywords: gas nitriding; accelerating methods; nitriding behavior; techno-economic



Citation: Zhou, Y.-L.; Xia, F.; Xie, A.-J.; Peng, H.-P.; Wang, J.-H.; Li, Z.-W. A Review—Effect of Accelerating Methods on Gas Nitriding: Accelerating Mechanism, Nitriding Behavior, and Techno-Economic Analysis. *Coatings* **2023**, *13*, 1846. <https://doi.org/10.3390/coatings13111846>

Academic Editor: Alexander Tolstoguzov

Received: 14 September 2023

Revised: 23 October 2023

Accepted: 23 October 2023

Published: 27 October 2023



Copyright: © 2023 by the authors. Licensee MDPI, Basel, Switzerland. This article is an open access article distributed under the terms and conditions of the Creative Commons Attribution (CC BY) license (<https://creativecommons.org/licenses/by/4.0/>).

1. Introduction

Mendoza et al. showed that as the demand for renewable energy continues to grow worldwide, wind power technology has become an important part of it [1–3]. In the wind power industry, wind turbines are the core equipment of wind power generation systems, and their performance has a crucial impact on the efficiency and reliability of the entire system. However, due to the long-term impact of the environment and the pressure of the operating load, wind turbines often face various engineering failure problems, such as mechanical fatigue, corrosion, etc. [4,5]. In order to solve these problems, engineers have been constantly exploring new technologies and methods. There are many ways to harden the surface of steel. Usually, different methods can be selected according to the required hardness, depth, and process, such as carburizing, nitriding, quenching, laser hardening, and chemical heat treatment. Carburizing is usually carried out by exposing carbon-containing substances (such as solid carbon powder or gas) to the surface of the steel at high temperatures, thereby forming a carbon-rich hardened layer on the surface. Carburizing can provide higher surface hardness and wear resistance. However, it requires a long processing cycle. It may lead to uneven distribution of surface carbon. And,

high-temperature treatment (850–950 °C) may lead to deformation and metamorphism. Quenching is an important metal treatment process, which can be used to change the properties of metals and improve their hardness and strength. Quenching has fast heating and cooling rates and is suitable for local hardening, but only for conductive materials. Laser hardening is a heat treatment process that uses a laser beam to locally heat the metal surface to increase the hardness and wear resistance of the metal. Laser hardening has the advantages of high heating accuracy, controllable depth, and no deformation. However, the equipment cost is high, requires highly trained operators, and is only suitable for local hardening. In contrast, gas nitriding is usually carried out at a lower temperature (500–580 °C), which does not change the chemical composition of the steel, and can be applied to the integrated nitriding of large or ultra-large workpieces [6]. As one of these technologies, gas nitriding can form an extremely hard nitrided layer on the surface of wind turbines to improve hardness and corrosion resistance [7,8]. In addition, gas nitriding technology can also improve the surface quality of wind turbine blades, reduce air resistance, and further improve its power generation efficiency [9–11]. In addition to wind turbines, gas nitriding technology is also widely used in other equipment in the wind power industry. For example, gas nitriding technology can improve the hardness and corrosion resistance of towers in wind farms and prolong their service life [12,13]. Due to the advantages of environmental protection and low cost, gas nitriding technology has been more and more widely used and promoted in the wind power industry [14–16].

Gas nitriding is a chemical heat treatment process which makes nitrogen atoms penetrate into the surface of the workpiece at a certain temperature and in a certain medium [17,18]. It generally includes three processes [19–21]: generation of active nitrogen atoms, surface absorption, and diffusion of nitrogen atoms. The surface of the workpiece after nitriding treatment usually has the characteristics of high hardness [22], good wear resistance [23], high fatigue strength [24], and excellent corrosion resistance [17]. However, the traditional nitriding temperature is high and the nitriding time is long, which not only wastes energy and increases the manufacturing cost of the workpiece but also causes some performance reduction in the workpiece. For example, if the nitriding temperature of stainless steel is too high, it will cause a lack of chromium in the substrate and the degradation of corrosion resistance [25–28]. For aluminum alloy workpieces, if the nitriding temperature is too high, the matrix structure will change significantly, which will lead to poor inherent properties [29,30]. In the nitriding process, the temperature affects the nitriding speed, the decomposition efficiency of the nitriding medium, and the structure of the nitrided layer [31,32]. CrMo steel is usually used to manufacture parts with high strength and high-temperature operation, such as boilers, pressure vessels, steam turbine components, etc. Gas nitriding can improve the hardness and wear resistance of CrMo steel, making it more suitable for use in high-stress and high-temperature environments. It can also improve the corrosion resistance and prolong the life of the parts. Nickel-based alloys are widely used in high-temperature and corrosive environments, such as the aerospace, petrochemical, and energy industries. Gas nitriding can improve the surface hardness and wear resistance of nickel-based alloys and improve their performance in high-temperature and corrosive environments. This helps to extend the service life of alloy parts. Cobalt-based alloys are commonly used in the manufacture of high-temperature, high-strength, and corrosion-resistant parts, such as aero-engine parts and chemical equipment. Gas nitriding can increase the hardness and wear resistance of cobalt-based alloys and improve their stability in high-temperature and corrosive environments. This is very important for extending the life of alloy parts. Cemented carbides are commonly used for cutting, drilling, grinding, and other cutting tools as well as wear-resistant parts, such as mechanical seals and bearings. Gas nitriding can increase the surface hardness and wear resistance of cemented carbide tools, thereby prolonging their service life. This can improve the performance of cutting tools and reduce downtime. The application of gas nitriding on different materials has a common goal, that is, to improve the hardness, wear resistance, and corrosion resistance of the material so as to increase the life and performance of the

parts. However, the specific effects may vary depending on the type of material and the environment in which it is used. Therefore, when choosing gas nitriding as a surface treatment method, it is necessary to adjust the nitriding parameters and processes according to the specific application requirements. In this review, in order to facilitate the technical and economic analysis, the CrMo steel used in wind turbine is selected as the target, and the effect and application of gas nitriding are described. How to carry out nitriding at low temperature has become a hot spot of international research.

The traditional method of gas nitriding has problems such as slow diffusion rate, high energy consumption, and uneven thickness of the infiltrated layer, which limits its application in industrial production [33,34]. The implementation of the “carbon peak, carbon neutral” strategy provides a strong driving force for the popularization and the application of nitriding wear-resistant and corrosion-resistant green surface treatment technology [35]. Improving the diffusion rate of gas nitriding is not only conducive to reducing energy consumption and achieving the goal of “carbon peak and carbon neutrality” but also can reduce production costs and expand the application field of nitriding technology. More and more scholars and researchers are conducting research on the new process of accelerating nitriding. Accelerating nitriding is a nitriding method that uses the accelerating method to promote the diffusion of nitrogen atoms on the metal surface, which can significantly increase the diffusion rate of nitrogen atoms and reduce nitriding time and energy consumption. It can also achieve uniform layer thickness and reduce residual stress at the same time [36]. Figure 1 shows the application of accelerating nitriding in the field of wind power. Among these processes, process parameter optimization [18,37,38], surface mechanical nano-crystallization [39–41], surface active catalysis [42–44], surface pre-oxidation [45–47], and surface laser treatment [48–50] are relatively common accelerating nitriding methods. The development of accelerating nitriding methods is also expected to expand its application in other fields. For example, nitriding technology has important application value in new energy materials [51,52], nano-materials [53,54], biomedicine [55,56], and other fields. Therefore, strengthening the research and development of accelerating nitriding methods will help to promote its application and promotion in industrial production and other fields.

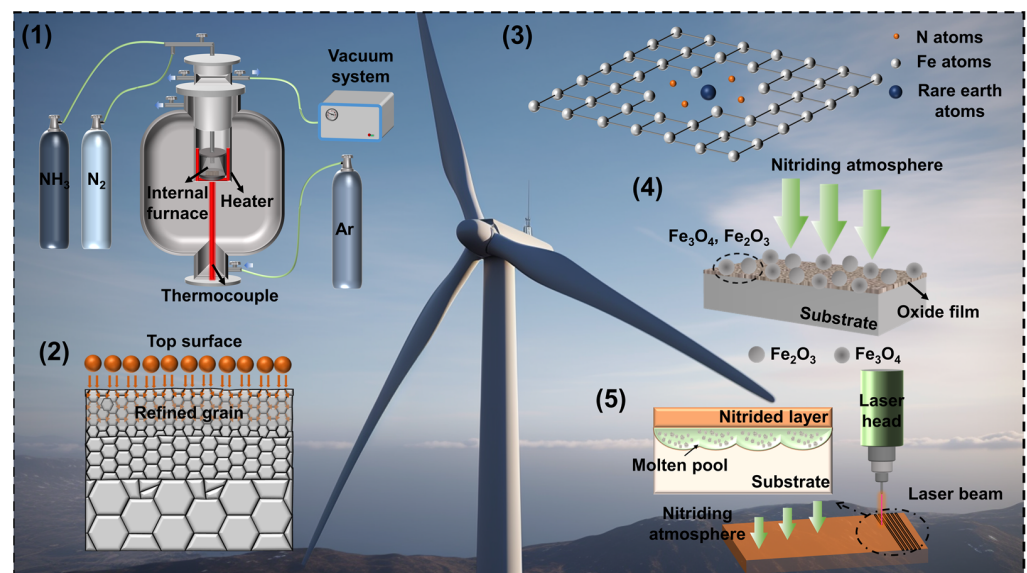


Figure 1. Application of accelerating gas nitriding in wind power field: (1) process parameter optimization, (2) Surface Mechanical Nano-Crystallization, (3) surface-active catalytic nitriding, (4) surface pre-oxidized nitriding, and (5) surface laser treatment.

Based on the above content, this review analyzes the accelerating nitriding mechanism of process parameter optimization, surface mechanical nano-crystallization, surface active catalysis, surface pre-oxidation, and surface laser treatment. In addition, this review

summarizes its effect on nitriding behavior and further analyzes the economic and environmental benefits and the technology readiness level of different accelerating nitriding methods. This review also predicts and surveys the application of gas nitriding in the wind power industry and the development trend of accelerating nitriding methods in the next 10 years. Overall, this review will play an important role in informing researchers, scholars, and policy makers and pave the way for future research studies and decision-making.

2. Research Progress of Conventional Gas Nitriding

2.1. Mechanism of Gas Nitriding

Gas nitriding is a surface strengthening technology that makes the nitriding atmosphere penetrate to the surface of metal or alloy material and diffuse to a certain depth under the conditions of high temperature and high pressure [48,57]. During gas nitriding, nitrogen atoms chemically react with metal surface atoms to form a nitrided layer that is hard, wear resistant, corrosion resistant, and metal fatigue resistant. Gas nitriding generally uses NH_3 , $\text{NH}_3 + \text{N}_2$, or $\text{NH}_3 + \text{H}_2$ as the gas medium [58]. Figure 2 shows the gas nitriding interface reaction process [20]. The whole nitriding process is divided into three stages: decomposition of NH_3 , adsorption of active N atoms ($[\text{N}]$), and diffusion of active N atoms ($[\text{N}]$) [19]. The ammonia gas entering the nitriding furnace cavity is divided into two parts: one part is directly thermally decomposed ammonia gas (NH_3^{D}), and the other part is undecomposed residual ammonia gas flowing through the surface of the workpiece in the form of NH_3 molecules (NH_3^{R}). Gas nitriding mainly depends on the interface reaction between the ammonia gas (NH_3^{R}) flowing through the surface of the workpiece [59]. It can be seen from Figure 2 that the effective infiltration of N atoms depends on the adsorption, decomposition, and absorption process of ammonia on the workpiece surface. The active N atoms generated by the thermal decomposition of NH_3^{R} participate in the nitriding reaction and diffuse into the substrate to form a nitrided layer and promote it to grow thicker [21,60,61]. Therefore, according to Figure 2, the basic mechanism of gas nitriding is analyzed from the physicochemical reaction, adsorption, and diffusion of active N atoms ($[\text{N}]$).

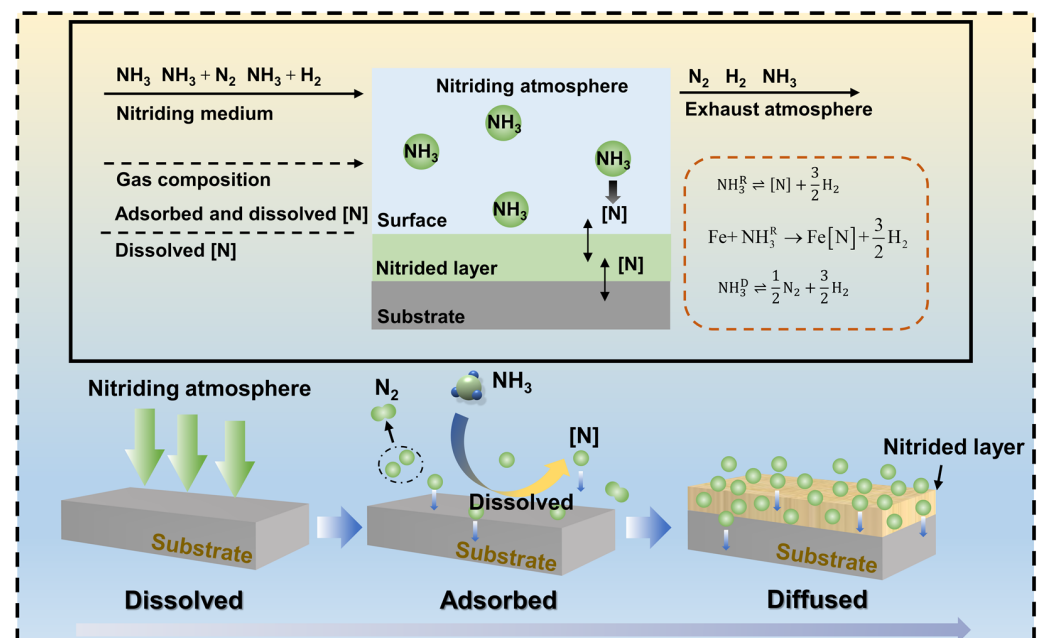


Figure 2. Interface reaction process of gas nitriding.

(1) Physicochemical reaction [58].

There are many physicochemical reactions in the gas nitriding process, mainly including the chemical reaction of the nitriding medium, the adsorption of active N atoms

on the surface of the workpiece, and the diffusion into the substrate. The ammonia gas decomposition reaction on the surface of workpiece during nitriding process is as follows:



(2) Adsorption and diffusion of active N atoms ([N]) [58].

During the nitriding process, active N atoms are adsorbed on the surface of the workpiece to form Fe[N] solid solution [19]. From the perspective of thermodynamic equilibrium [62,63], due to the concentration difference in nitrogen between the surface and the metal substrate, N atoms will diffuse directionally into the grains inside the substrate. Due to the change in factors such as nitriding temperature and time, the diffusion of active N atoms is accompanied by phase transformation during the nitriding process, mainly including diffusion [64], phase transformation diffusion [65,66], and reaction diffusion [62,67].

2.2. Nitrided Layer Structure of Gas Nitriding

Gas nitriding forms a surface layer with a high nitrogen concentration on the surface of metal by exposing metal samples to reactive gases such as nitrogen. This surface layer is called the nitrided layer [68].

The nitrided layer usually consists of two regions: the case-hardened layer and the hardened layer. The case-hardened layer is usually located on the surface of the nitrided layer and consists of a solid solution with a high nitrogen concentration. The hardened layer is located below the case-hardened layer and consists of solid solutions and nitrides with a relatively low nitrogen concentration. The hardened layer has higher toughness and strength, while the case-hardened layer has higher hardness [69].

During the nitriding process, the interaction of Fe and N can be analyzed through the phase diagram of the Fe-N binary alloy (as shown in Figure 3) [70]. The phase diagram includes two interstitial solid solutions, α and γ , and three interstitial phases, γ' , ϵ , and ζ . There are two eutectoid transitions in the phase diagram: at 592 °C and 2.4 wt.% N, the $\gamma \rightarrow \alpha + \gamma'$ eutectoid transition occurs; at 650 °C and 4.5 wt.%, $\epsilon \rightarrow \gamma + \gamma'$ eutectoid transformation occurs. The phase diagram of the Fe-N binary alloy shows that the mutual solubility of Fe and N is extremely low, and the solid solution can only be formed under high-temperature and high-pressure conditions. At room temperature, the nitrided layer is mainly composed of two phases: a nitride phase and a retained austenite phase. The nitride phase mainly includes Fe_4N , Fe_3N , and Fe_2N [71]. Among them, Fe_4N has the best thermal stability and is most commonly used in the nitriding process [64]. The retained austenite phase is mainly unnitrided austenite structure. The crystal structure of each phase is analyzed separately as follows:

The α phase belongs to the retained austenite phase of the nitrided layer. It is an interstitial solid solution of N in α -Fe, also known as nitrogen-containing ferrite. The lattice structure is a body-centered cubic structure and N atoms are located in the octahedral gap in the α -Fe lattice.

The γ phase belongs to the nitride phase in the nitrided layer. It is an interstitial solid solution of N in γ -Fe, also known as nitrogen-containing austenite. The lattice structure is a face-centered cubic structure, and N atoms are randomly distributed in the octahedral gaps in the γ -Fe lattice. The γ phase undergoes eutectoid reaction at 592 °C. Eutectoid decomposition occurs during slow cooling. $\gamma \rightarrow \alpha + \gamma'$ eutectoid decomposition occurs during slow cooling. During rapid cooling, $\gamma \rightarrow \alpha'$ transformation occurs, and the γ' phase transforms into nitrogen-containing martensite (α' phase) or exists in the state of retained austenite.

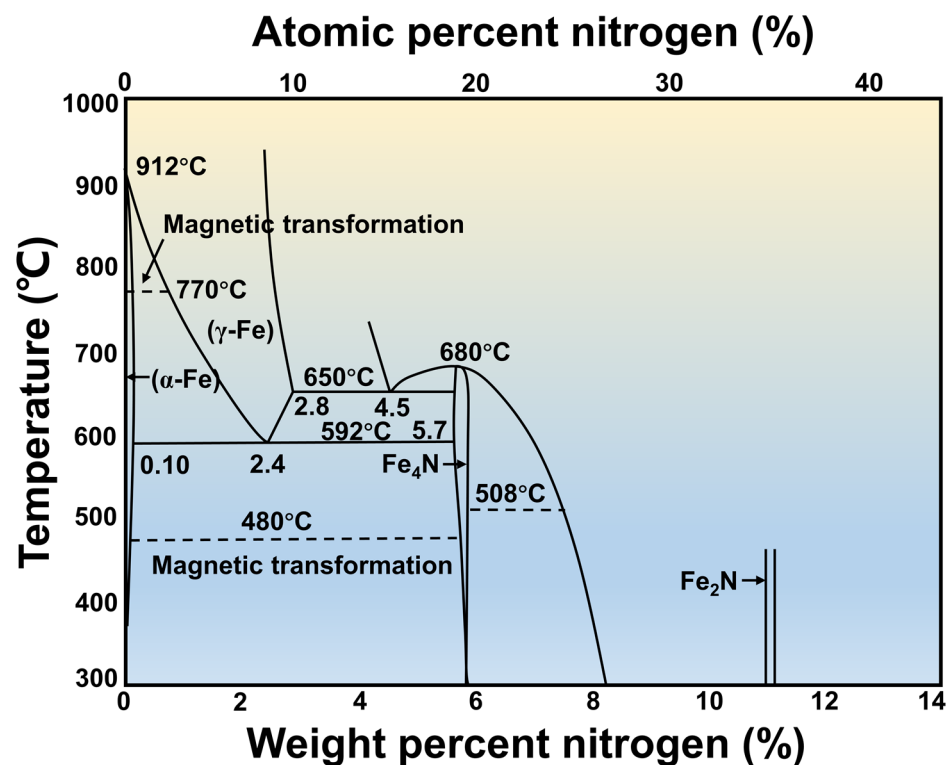


Figure 3. Phase diagram of Fe-N binary alloy.

The γ' phase, an interstitial phase with a nitrogen content between 5.7 wt.% and 6.1 wt.% and a variable composition, is represented by γ' -Fe₄N. γ' -Fe₄N has a stable structure, and N atoms orderly occupy the interstitial positions of the face-centered cubic lattice composed of Fe atoms. When the temperature is above 680 °C, it will decompose and transform into ϵ -Fe_{2.3}N.

The ϵ phase belongs to the nitride phase in the nitrided layer. It is a solid solution based on Fe₃N, represented by ϵ -Fe_{2.3}N. In the compound, N atoms orderly occupy the gaps of the close-packed hexagonal lattice composed of Fe atoms. The ϵ phase is a ferromagnetic phase, and the eutectoid decomposition of $\epsilon \rightarrow \gamma + \gamma'$ occurs at 650 °C.

The ζ phase belongs to the nitride phase in the nitrided layer. It is a kind of interstitial solid solution based on Fe₂N compound with an orthogonal rhombic lattice and nitrogen content between 11.07–11.18 wt.% and is brittle. The ζ phase transforms into the ϵ -Fe_{2.3}N phase above 520 °C.

2.3. Process Parameters of Gas Nitriding

The process parameters that affect the efficiency of gas nitriding are mainly nitriding temperature, nitriding time, atmosphere pressure, and NH₃ flow rate. These parameters complement each other in the nitriding process.

(1) Nitriding temperature is an important parameter in the gas nitriding process, which will have a significant impact on the formation and the performance of the nitrided layer. Usually, the nitriding temperature is between 450 and 580 °C. If the temperature is too high, it will lead to excessive nitride formation, which will make the nitrided layer brittle. However, for stainless steel, although increasing the nitriding temperature can increase the thickness of the nitrided layer, it will also cause thermal decomposition of the γ _N-Fe phase and reduce the corrosion resistance of stainless steel, which is not advisable [72,73]. Studies have shown that the nitriding rate increases with the increasing temperature within a certain range. However, the depth of the nitrided layer shows a trend of increasing first and then decreasing, and there is an optimal temperature range. This is due to the fact that the growth of the nitrided layer is limited by solid-phase diffusion and liquid-phase diffusion [74].

For example, Chen et al. [75] state that during nitriding, the optimum temperature is 560–580 °C. Beyond this range, both the depth and hardness of the nitrided layer will decrease. The nitriding temperature also affects the structure and the performance of the nitrided layer. A higher temperature is conducive to the formation of a dense nitrided layer, improving its hardness and wear resistance, but too high a temperature will also lead to the coarsening of the grains of the nitrided layer and the formation of cracks [76]. In addition, the nitriding temperature will also affect the chemical reaction and the affinity between the nitrided layer and the substrate, thereby affecting its bonding strength and corrosion resistance [77]. For example, Xiang et al. [78] found that nitriding at low temperatures resulted in a denser nitrided layer, improving its corrosion resistance and fatigue life.

(2) Nitriding time: Exposure time of metal samples in nitriding atmosphere. Typically, the nitriding time is between 2 and 48 h, depending on the type of material, size, and desired nitriding depth. Generally speaking, a longer nitriding time is conducive to the formation of a dense nitrided layer, which improves its hardness and wear resistance. However, too long a nitriding time will also lead to grain coarsening and surface roughness of the nitrided layer [79,80].

The relationship between the thickness of the nitrided layer and the diffusion time is shown in formula (3) [72]. Assuming that the diffusion coefficient remains consistent, the thickness of the nitrided layer of the nitriding workpiece increases with the increase in the diffusion time.

$$X \propto \sqrt{Dt} \quad (3)$$

where X is the thickness of the nitrided layer (m), D is the diffusion coefficient (m^2/s), and t is the diffusion time (s). But for stainless steel, too long a nitriding time will also cause thermal decomposition of the γ_{N} -Fe phase and reduce the corrosion resistance of stainless steel, so this is not advisable [73].

(3) Atmospheric pressure is also one of the important parameters affecting nitriding. Usually, the pressure during nitriding is between 0.1 and 2.0 MPa. As the atmosphere pressure increases, the nitriding rate and penetration depth gradually increase [81]. Wang et al. [20] pointed out that during nitriding, the atmospheric pressure increased from 0.1 MPa to 0.5 MPa, and the penetration depth increased from 0.21 mm to 1.1 mm. A higher atmospheric pressure can increase the penetration depth and the nitriding rate, which is conducive to the formation of a dense nitrided layer and improves its hardness and wear resistance.

(4) Nitrogen flow: When gas nitriding, the flow rate of nitrogen is also an important parameter, it is usually between 5 L/min and 50 L/min [82]. Michalski et al. [83] pointed out that an increase in nitrogen flow can significantly increase the nitriding rate and the depth of the nitrided layer. In this study, gas nitriding treatment was performed on magnesium alloy by changing the nitrogen flow rate, and the results showed that when the nitrogen flow rate increased from 10 L/min to 30 L/min, the nitriding rate increased from 0.47 $\mu\text{m}/\text{h}$ to 1.47 $\mu\text{m}/\text{h}$, and the depth of the nitrided layer increased from 16.2 μm to 51.6 μm . However, when the nitrogen flow rate is too high, it will cause excessive accumulation of nitrogen atoms in the nitrided layer, forming pores and cracks, thereby reducing the quality of the nitrided layer [84]. Excessive nitrogen flow will also increase the consumption of nitrogen, thereby increasing the cost of nitriding. Therefore, in actual production, it is necessary to adjust the nitrogen flow rate to find the best nitriding process parameters to obtain a high-quality nitrided layer.

(5) Nitriding media [85]: there are many types of nitriding media, and the common ones are as follows:

Ammonia: Ammonia is one of the most commonly used nitriding media in gas nitriding. It can realize high-speed nitriding at a lower temperature and form a uniform nitrided layer. Ammonia can also control the depth and the hardness of the nitrided layer by adjusting the temperature and ammonia flow. However, ammonia gas is toxic and flammable and requires special safety measures during nitriding.

Nitrogen: Nitrogen is an inert gas that can be used as a nitriding medium for nitriding. The rate of nitrogen nitriding is slow, requiring higher temperature and longer time to achieve a certain depth of nitrided layer. However, nitrogen has the advantages of stability and safety and will not have adverse effects on the human body and the environment.

Mixed composition: Mixed gas refers to the nitriding medium that mixes different gases, such as ammonia and nitrogen, in a certain proportion. The mixed gas can combine the advantages of ammonia and nitrogen, can realize high-speed nitriding at lower temperature and time, and can control the depth and the hardness of the nitrided layer. However, the cost of mixed gas is relatively high.

In addition to the above common nitriding media, there are other nitriding media, such as argon, hydrogen, etc. Selecting a suitable nitriding medium needs to consider specific application scenarios and requirements, such as nitriding rate, nitriding depth, cost, and other factors.

3. Effect of Accelerating Nitriding Methods on the Behavior and Efficiency of Gas Nitriding

3.1. Process Parameter Optimization

3.1.1. Accelerating Nitriding Mechanism of Optimizing Process Parameters

Nitriding workpieces are required to have a hard and tough nitrided layer under actual service conditions, which mainly depends on the structure of the nitrided layer (γ' phase and ε phase). The porous ε phase is the main cause of embrittlement and spalling of the nitrided layer. Therefore, controlling the composition of the white layer of the nitrided layer or making the white layer disappear is the focus of research [81,86].

Some scholars put forward the concept of controllable nitriding, which was called computer-controlled gas nitriding [87]. Based on Lehrer's point of view (Figure 4a), using the relationship between the limit nitrogen potential and temperature (Equation (6)) [34,88], a computer-controlled, fully industrially automated gas nitriding control system has been designed and applied successfully. Its commercial registration name is NITREG [89]. Michalski et al. [88] used controllable gas nitriding (NITREG[®]) to obtain a nitrided layer containing only γ' -Fe₄N-phase nitrides on the surface of carbon steel. Subsequently, the team used this method to prepare dense compound layers and nitrided layers without compound layers on the surface of 40HM and 38HMJ steels. Among them, the nitrided layers of 40HM and 38HMJ steels without compound layers showed the highest hardness values, respectively >700 HV_{0.5} and 1100 HV_{0.5} [37].

After controlled gas nitriding treatment of 42CrMosteel, Panfil et al. [90] used laser heat treatment to modify the compound layer instead of remelting and found that the porosity of the porous and brittle compound layer can be reduced, and the indentation modulus (165.72 ± 18.67 GPa) and hardness (9.90 ± 0.47 GPa) of the ε -Fe₂₋₃N area can be improved.

$$K_N \gamma' / \varepsilon = \left[\exp\left(\frac{60536}{T} - 56.85\right)^{0.5} - 9.63 \right] \times \left(1.013 \times 10^5\right)^{0.5} \quad (4)$$

where $K_N \gamma' / \varepsilon$ is the limiting nitrogen potential ($\text{atm}^{-1/2}$), and T is the nitriding temperature (K).

The nitrogen potential (K_N) is one of the factors to be considered in the study of the growth kinetics of the nitrided layer, which can be calculated by the following formula [21]:

$$K_N = \frac{P_{NH_3}}{(P_{H_2})^{1.5}} \quad (5)$$

where P_{NH_3} is the partial pressure of ammonia in the atmosphere, and P_{H_2} is the partial pressure of hydrogen in the atmosphere. The nitriding pressure affects the interface reaction rate, the surface nitrogen potential, and the growth of the nitrided layer. NH_3 flow affects the ammonia decomposition rate and is also an important means to change the nitrogen

potential on the workpiece surface. The relationship expression between nitrogen potential and ammonia decomposition rate (ω) is as follows [82]:

$$K_N = \frac{1 - \omega}{(0.75\omega)^{1.5}} \tag{6}$$

Figure 4b shows the relationship between the nitrogen production rate of ammonia decomposition and the ammonia content in the furnace atmosphere and the ammonia gas flow into the furnace [91].

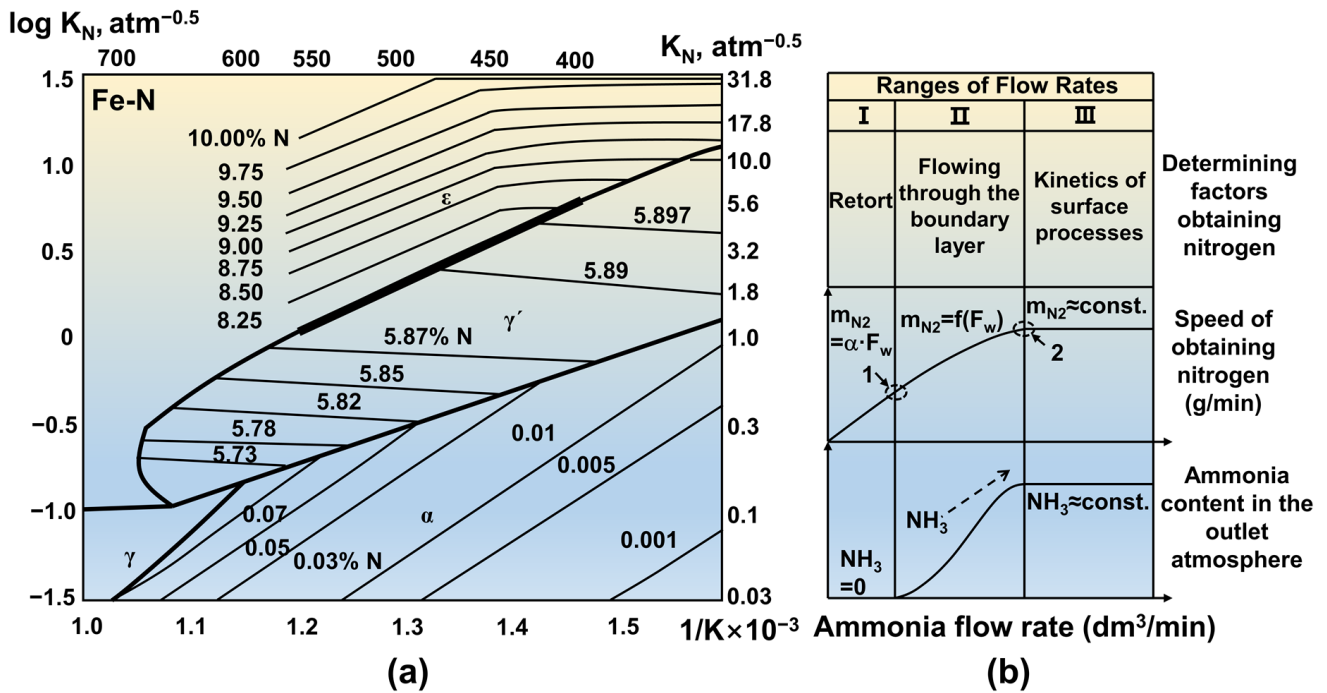


Figure 4. (a) Lehrer Fe–N equilibrium phase diagram and (b) the relationship between ammonia decomposition nitrogen production and ammonia content in the furnace atmosphere and the flow rate of ammonia gas flowing into the furnace.

In the first stage, the flow rate of ammonia gas is very small. The rate of nitrogen production is proportional to the flow rate of ammonia gas entering the furnace, and the atmosphere out of the furnace only contains the decomposition products of ammonia. With the further increase in the ammonia gas flow rate to point 1, the contact time between the ammonia molecules and the workpiece surface is so short that some of the ammonia molecules cannot be decomposed. Therefore, the atmosphere of the furnace is nitrogen, hydrogen, and ammonia.

In the second stage, the nitrogen production rate is mainly determined by the ammonia content on the surface of workpiece. The rate of nitrogen production increases with the increase in the ammonia flow rate and tends to be stable at point 2.

When the flow of ammonia gas enters the third stage, the yield of nitrogen remains constant, and the amount of nitrogen produced is determined by the reaction kinetics (adsorption, desorption, and chemical adsorption) on the surface of the workpiece [82]. This shows that it is meaningless to study the nitrogen potential in stage III.

The nitrogen potential (K_N) is one of the factors to be considered in the study of the growth kinetics of the nitrated layer. As shown in Equations (4) and (5), the nitrogen potential is determined by temperature and pressure. Therefore, the effects of process parameters on gas nitriding and nitriding behavior are introduced from the two aspects of pressure and temperature.

3.1.2. Effect of Process Parameter Optimization on Nitriding Behavior

Effect of Pressure on Nitriding Behavior

Pressure is one of the factors affecting nitriding efficiency. From the ammonia decomposition formula, it can be seen that increasing the pressure can inhibit the decomposition of ammonia, reduce the decomposition rate of ammonia, and increase the nitrogen potential [81]. Fu et al. [71] developed a special pressurized gas equipment—a new type of gas nitriding furnace with a dual-pressure balance structure. The schematic diagram of the equipment is shown in Figure 5a. NH_3 and Ar at the same pressure are fed into the inner furnace and outer furnace, respectively, and the pressure in the reaction chamber can be adjusted in a wide range by balancing the pressure of the inner and outer layers of the inner furnace wall to realize high-pressure gas nitriding. The equipment can ensure the smooth progress of the gas nitriding within the pressure range of 0–1.0 MPa.

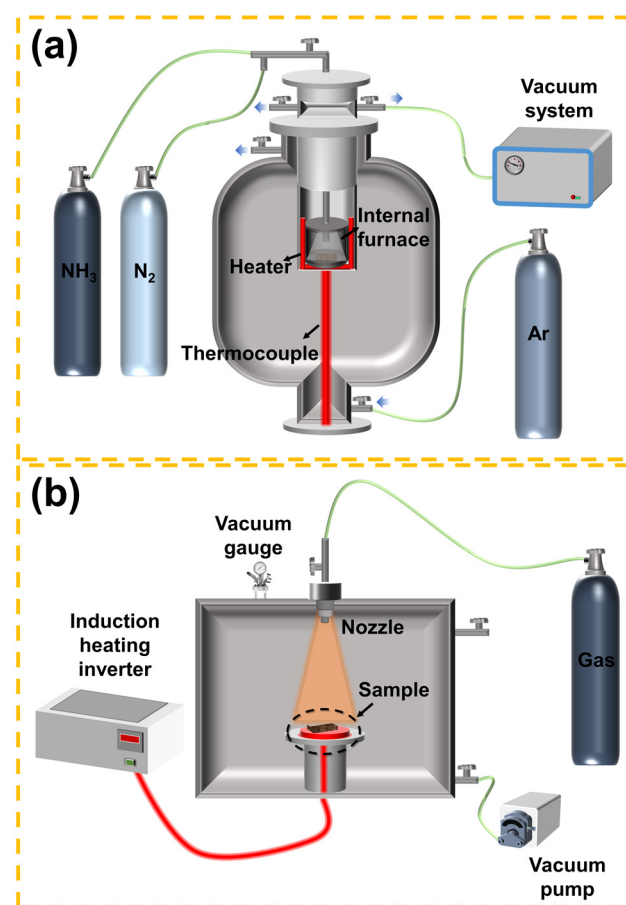


Figure 5. (a) Simplified diagram of pressurized gas nitriding equipment. (b) Schematic diagram of gas-blown induction heating (GBIH) nitriding plant.

Wang et al. [71] used NH_3 as the medium to study the gas nitriding behavior of 38CrMoAl steel under the conditions of 510 °C and 1–6 atm. It was found that with the increase in pressure, the phase of the nitrided layer transforms as follows: a large amount of γ' - Fe_4N + a small amount of ϵ - Fe_{2-3}N + α -Fe \rightarrow γ' - Fe_4N + ϵ - Fe_{2-3}N \rightarrow γ' - Fe_4N + α -Fe. With the increase in the pressure, the surface hardness of the nitrided sample first increases and then decreases and reaches a maximum value of about 1170 HV at 3.5 atm. At 6 atm, the thickness of the nitrided layer is as high as 410 μm , and the wear resistance is the best. Subsequent research also found that under the condition of 1–5 atm, the thickness of the nitrided layer can be increased from 210 μm to 1100 μm by gas nitriding treatment of pure iron at 500 °C for 5 h. When the nitriding pressure increases from 1 atm to 3 atm, the

thickness of the compound layer increases from 5.3 μm to 10 μm , and then the thickness of the compound layer tends to be stable without being affected by the nitriding pressure. When the nitriding pressure increased from 1 atm to 3 atm, the phase ratio of the $\epsilon\text{-Fe}_{2-3}\text{N}$ phase and $\gamma'\text{-Fe}_4\text{N}$ phase increased. When the nitriding pressure continues to increase to 5 atm, the phase ratio of the $\epsilon\text{-Fe}_{2-3}\text{N}$ phase and $\gamma'\text{-Fe}_4\text{N}$ phase shows a downward trend. When the nitriding pressure is 3 atm, the phase ratio of the $\epsilon\text{-Fe}_{2-3}\text{N}$ phase and $\gamma'\text{-Fe}_4\text{N}$ phase is the highest. These show that the composition of the compound layer can be controlled by controlling the nitriding pressure [20].

Effect of Temperature on Nitriding Behavior

For most steels, temperature is one of the main factors affecting the phase composition and properties of the nitrided layer. The temperature range of gas nitriding is generally 400–570 $^{\circ}\text{C}$. The higher the temperature is, the deeper the nitriding layer is, but if it exceeds 550 $^{\circ}\text{C}$, the nitrides will aggregate and grow to reduce the hardness [92]. Yazici et al. [93] found that when the nitriding temperature is higher than 450 $^{\circ}\text{C}$, the corrosion resistance of the nitrided layer decreases due to the formation of chromium nitride. Therefore, the nitriding temperature should not be too high.

Xi et al. [94] used X-ray diffraction (XRD) to study the phase composition and evolution of the nitrided layer of martensitic stainless steel and concluded that low-temperature nitriding formed N-supersaturated α_{N} phase and $\epsilon\text{-Fe}_{2-3}\text{N}$ nitride, which made the hardness and wear resistance greatly improved. When the nitriding temperature is raised, the α_{N} phase gradually transforms into α phase and CrN phase, forming a nitrided layer composed of α , $\epsilon\text{-Fe}_{2-3}\text{N}$, $\gamma'\text{-Fe}_4\text{N}$, and CrN, which reduces the hardness of the nitrided layer.

Shogo et al. [95] used a nitriding device to characterize the surface modification layer of Ti-6Al-4V alloy produced by gas-blown induction heating (GBIH). The schematic diagram of the device is shown in Figure 5b. The device studies the effect of temperature on nitriding behavior by monitoring the internal temperature of the material, the electrical effect generated by induction heating (IH), nitrogen gas blowing, and the effect of passivation film on titanium alloys. It was found that the nitrided layer obtained by GBIH nitriding was thicker than that calculated from the diffusion coefficient inside the sample at high temperature. This is because during the nitriding process of GBIH, the electric effect generated by IH makes part of the nitrided layer to form rapidly. The electric effect of IH can also make the passivation film on the surface of Ti-6Al-4V alloy disappear rapidly during the GBIH nitriding process. Since the GBIH nitriding treatment is carried out under the condition of controlled atmosphere, the passivation film on the surface of the alloy will not be regenerated. Only a few minutes of GBIH nitriding can form nitrided layers on the surface of Ti-6Al-4V alloy, and the characteristics of these nitrided layers are similar to those formed after several hours of ordinary gas nitriding [96–98]. GBIH nitriding can modify Ti-6Al-4V alloy in a short time, mainly due to the electrical effect and the disappearance of passivation film produced by nitriding.

3.1.3. Effect of Process Parameter Optimization on Nitriding Efficiency

The influence of process parameter optimization on nitriding efficiency was compared and analyzed from the four aspects of nitriding time, nitriding temperature, nitriding layer structure, and nitriding layer hardness. According to the literature summary, and after taking the average value, the comparison histogram of parameter optimization gas nitriding and conventional gas nitriding efficiency uniformity is obtained, as shown in Figure 6.

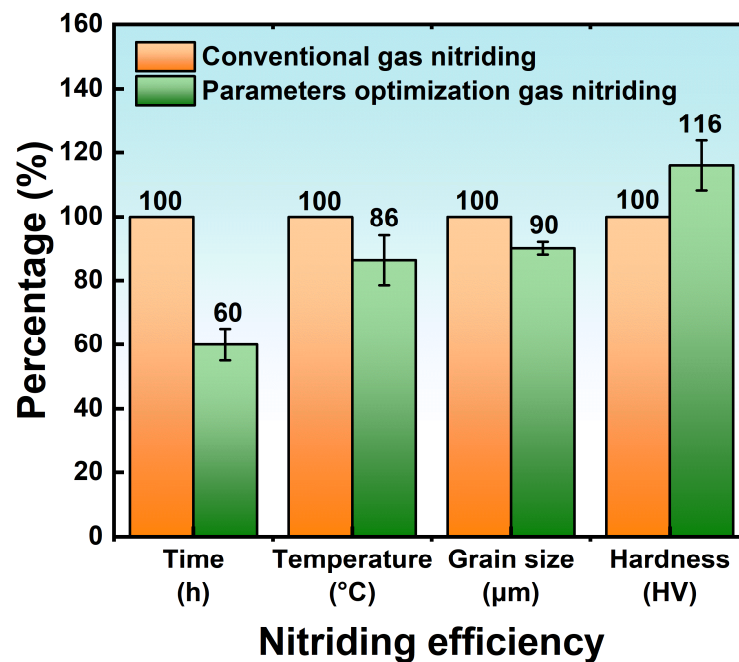


Figure 6. Histogram of efficiency comparison between parameter-optimized gas nitriding and conventional gas nitriding.

(1) Nitriding time: Increasing temperature and pressure can shorten nitriding time by 60%. Lu et al. [99] found that the nitriding time of 304 stainless steel can be shortened from 8 h to 3 h under the condition of increasing temperature and pressure. Similarly, Alekseeva et al. [22] also found that under the conditions of increasing temperature and pressure, the nitriding time of martensitic steel can be shortened from 15 h to 6 h. Therefore, the nitriding time of gas nitriding can be shortened and the production efficiency can be improved by increasing the temperature and pressure without affecting the quality of the nitriding layer.

(2) Nitriding temperature: Increasing the atmospheric pressure can reduce the nitriding temperature of gas nitriding to 86%. Wang et al. [71] found that the nitriding temperature of 38CrMoAl steel can be reduced from 600 °C in conventional processes to 500 °C under the condition of increasing the atmospheric pressure. Similarly, Wen et al. [100] also found that increasing the pressure can reduce the nitriding temperature of TC4 titanium alloy from 560 °C in conventional processes to 530 °C. Therefore, the nitriding temperature of gas nitriding can be reduced, the formation of the nitriding layer can be promoted, and its performance can be improved by increasing the atmospheric pressure.

(3) Nitrided layer structure: By optimizing the temperature and pressure, a better infiltrated structure can be obtained, and the grains are refined to 90%. Avelar-Batista et al. [101] found that a denser and more uniform infiltrated layer structure can be obtained through the multi-step glow discharge plasma technology. Similarly, Wang et al. [102] found that a denser and smoother layer structure can be obtained, and the corrosion resistance of the layer can be improved by increasing the pressure and time of gas nitriding. In addition, Fu et al. [20] also found that a denser and uniform nitrided layer structure can be obtained, and the thickness of the nitrided layer will increase accordingly under the conditions of increasing temperature and pressure. Therefore, the structure of the gas nitriding layer can be improved, and a denser layer can be obtained by optimizing the temperature and pressure.

(4) Nitrided layer hardness: The hardness of the gas nitriding layer can be increased to 116% by optimizing temperature and pressure [103,104]. Godec et al. [105] found that when the atmosphere ratio is 1:1, the hardness of the nitrided layer can reach 900 HV under the condition of 600 °C and 0.1 MPa. However, when the temperature rises to 700 °C, the hardness of the nitrided layer can reach more than 1000 HV. Michla et al. [106] found

that the hardness of the nitrided layer can reach 1100 HV under the conditions of 700 °C and 4.5 MPa. Therefore, a higher hardness of the nitrided layer can be obtained, and the hardness of the nitrided layer can reach more than 1000 HV by optimizing the temperature and pressure.

3.2. Surface Mechanical Nano-Crystallization

3.2.1. Accelerating the Nitriding Mechanism of Surface Mechanical Nano-Crystallization

Surface mechanical nano-crystallization (SMAT) is a method of using mechanical impact to cause strong plastic deformation on the surface of the material at a high strain rate, thereby forming nano-scale grains on the surface while there is no impurity pollution inside the metal material [107]. Generally, mechanical processing or heat treatment methods, such as shot blasting and surface mechanical abrasion treatment, are used to realize surface self-nano-crystallization on the metal surface, and to obtain the gradient nano-structure surface layer whose grain size gradually increases along the thickness direction [108].

Although the preparation methods of surface deformation nano-scale are different, the mechanism of surface grain refinement and strengthening is basically the same. Both use specific mechanical methods to increase the free energy of the metal material surface, so that the surface of the material undergoes strong plastic deformation at a high strain rate, thereby forming sub-grain boundaries, small-angle grain boundaries, dislocations, and twins within the grains. And, there is an interaction between them to divide the large grains on the metal surface to refine the grains, thereby realizing the nano-crystallization of the surface layer [109]. Based on the observation of the microstructure, it is found that when the metal material is deformed to produce grain refinement, the following process generally occurs: (1) formation of high-density dislocation walls (DDWs) and dislocation tangles (DTs) in the original grains; (2) high-density dislocation wall and transformation of dislocation entanglements into single crystals or sub-grains separated by low-angle grain boundaries; (3) sub-grain boundary evolves into high-angle grain boundary [110,111]. The mechanism of grain refinement is shown in Figure 7.

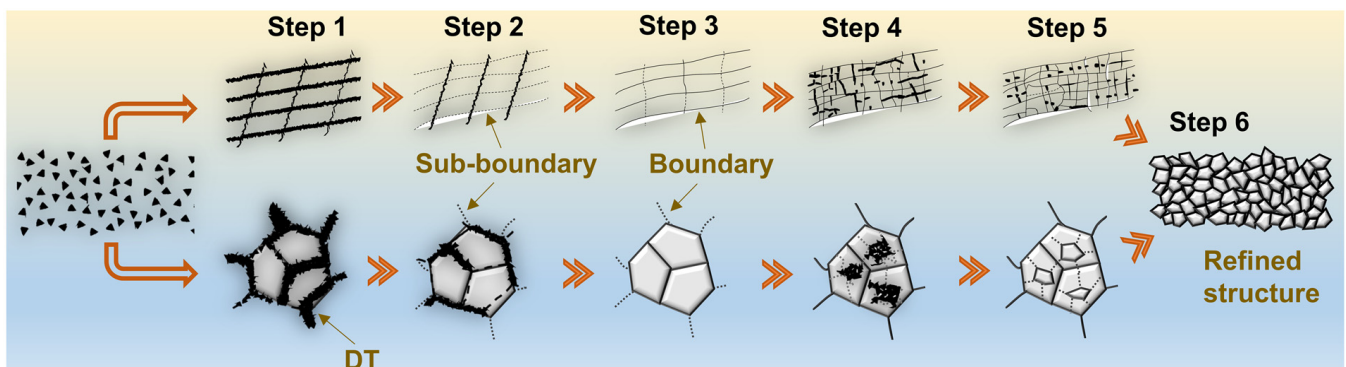


Figure 7. Grain refinement mechanism diagram of surface mechanical nano-crystallization.

When the metal surface is treated by mechanical methods, a certain stress field will be formed on the surface of the material, and the farther the depth from the surface is, the smaller the strain and strain rate will be. Therefore, the available structure of the metal material surface layer is a nano-crystalline, submicron crystalline layer, micron crystalline layer, and plastically deformed coarse crystalline transition layer. The grain size shows a gradient change law that gradually increases with the direction of depth change [109]. The formation of this surface nano-layer and the introduction of compressive stress can improve the corrosion resistance, friction and wear, and fatigue properties of the materials. It also has a good improvement effect on other surface treatment (such as chemical heat treatment, spraying, etc.) or interface bonding problems [112].

In general, nitrogen atoms require less activation energy for diffusion at dislocations or grain boundaries [19,113]. After plastic deformation on the surface of the metal workpiece,

the crystal grains can be refined, the short-circuit diffusion path can be increased, the nitriding temperature can be significantly reduced, and the infiltration rate of nitrogen atoms can be increased [114,115]. The surface mechanical deformation nano-structure can form a gradient nano-structure on the surface of the workpiece, which has a significant effect on promoting the nitriding process of the surface of the metal material. The surface mechanical nano-technology is simple and convenient and has been applied to the pretreatment of nitriding parts [107].

Since Lu [108] proposed the improvement of low-temperature nitriding technology by surface mechanical nano-technology, it has attracted extensive attention and exploration of international scholars and been applied to the pretreatment of various gas nitriding processes.

3.2.2. Effect of Surface Mechanical Nano-Crystallization on Nitriding Behavior

The formation of the nitrided layer in the gas nitriding process begins at certain energy-rich places, such as grain boundaries, surface defects and impurities, etc. [113]. As shown in Figure 8, unlike the substrate nitriding, the metal surface nano-layer has a high density of grain boundaries, such as dislocations, twins, and sub-grain boundaries, which provide ideal diffusion channels for N atoms [114]. The density of the lattice defects is also one of the conditions affecting the thickness of the nitrided layer. The nano-sized surface increases the grain boundary defects, provides an ideal channel for the diffusion of N atoms, significantly reduces the activation energy of N atom diffusion, and improves the nitriding kinetics [115].

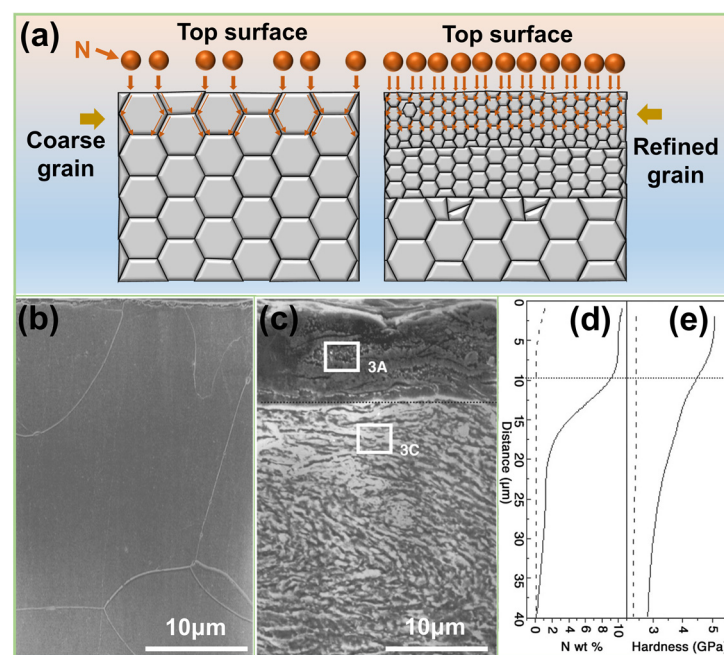


Figure 8. (a) A schematic diagram of the mechanism of the effect of surface mechanical nano-crystallization on gas nitriding behavior. (b) Cross-sectional micromorphology of the original coarse-grained iron sample after nitriding at 300 °C for 9 h. (c) Cross-sectional micromorphology of SMAT nitriding sample after nitriding at 300 °C for 9 h. (d) Nitrogen concentration, Original coarse-grained iron sample (dotted line), SMAT nitriding sample (solid line). (e) Microhardness, Original coarse-grained iron sample (dashed line), SMAT nitrided sample (solid line) [107]. Adapted with permission from [107], copyright 2003 AAAS.

Tong et al. [107] carried out nitriding for 9 h on an iron plate subjected to SMAT and an untreated iron plate in an NH_3 environment at 300 °C. The iron plate structure used in the experiment was α -Fe and the grain size was 100 μm. As shown in Figure 9, the α -Fe-phase grains on the surface of the SMAT sample still maintain nano-meter size, and

there is a nitrided layer with a thickness of about 10 μm on the surface, which is composed of $\epsilon\text{-Fe}_{2-3}\text{N}$ and $\gamma'\text{-Fe}_4\text{N}$ mixed phase and a small amount of $\alpha\text{-Fe}$ -phase composition, while the untreated sample is only composed of nitride and $\alpha\text{-Fe}$ -phase mixture. Compared with the untreated sample, the surface hardness of the SMAT sample increased, the friction coefficient decreased, and the wear resistance improved. This is mainly due to the existence of surface nano-crystals, which provide a large number of grain boundaries and other metallurgical structural defects, which effectively promote the diffusion of N atoms [116,117]. Compared with the intragranular diffusion, the activation energy of the grain boundary of Fe nano-crystals is only about half that of the intragranular, which is more conducive to the diffusion of N atoms. In addition, after mechanical grinding induces the surface nano-scale, a large amount of stored energy is formed at the grain boundary and within the grain, which provides an additional driving force for the nitriding process and promotes the formation of nitrides and the progress of low-temperature nitriding [118].

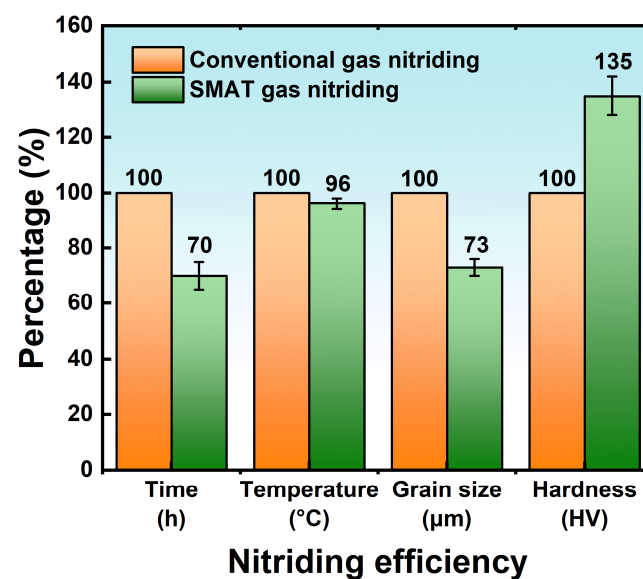


Figure 9. Histogram of efficiency comparison between surface mechanical nano-crystallization gas nitriding and conventional gas nitriding.

SMAT nitrided specimens have a thicker compound layer, a unique transition zone, and a diffuse layer with a small amount of acicular nitride. This excellent nitrided layer structure makes the SMAT nitrided samples show more excellent hardness and wear resistance [19,115]. Subsequent studies have also found that SMAT can also increase the thickness of the steel layer and accelerate the rate of nitride formation [119,120]. And, for the Cr-containing steel, a small amount of Fe_4N phase was formed in the SMAT nitrided sample, which was due to the high-temperature-induced nitride nucleation.

Sun et al. [121] used surface grinding treatment to prepare a nano-Ti layer on the surface of the Ti/Al composite sheet and found that the nitriding temperature of the SMAT sample was significantly lower compared with the traditional nitriding process. Compared with coarse-grain nitriding samples, SMAT nitriding samples generate thicker supersaturated $\epsilon\text{-TiN}$ and $\gamma\text{-Ti}_2\text{N}$ nitride layers (4 μm) at the interface of the Ti layer and Al layer. The wear resistance and corrosion resistance of the sample are also significantly improved. Chemkhi et al. [122] found that the nitrided layer of the SMAT sample increased from 26 μm to 40 μm after nitriding treatment at 425 $^\circ\text{C}$ for 20 h when the grain size was 50 nm.

Balusamy et al. [123] found that the increase in martensite content and the decrease in surface roughness are conducive to the diffusion of nitrogen atoms, promote the precipitation of the element Cr, and form a higher content of CrN. Moreover, a passivation layer with a thickness of 60–120 nm is formed. The formation of this type of passivation layer will inevitably have a great impact on the corrosion resistance of the sample. Lin [124]

and Zhang [125] found that compared with untreated nitriding samples, the wear life of SMAT-treated nitriding samples was 3 to 10 times that of untreated samples. This is because SMAT pretreatment promotes the formation of a nitrided layer and a gradient diffusion layer, which makes SMAT nitrided samples have higher hardness and bearing capacity.

In summary, the surface mechanical nano-technology can effectively promote the nitriding process on the surface of metal materials, reduce the nitriding temperature, increase the thickness of the nitriding layer, reduce the nitride crystal size, increase the nitride content, and improve the composite modified layer's performance.

The surface mechanical nano-crystallization and nitriding post-treatment composite modification layer is composed of a nitride layer, a diffusion layer accompanied by plastic deformation, and an undeformed diffusion region [123–125]. The mechanism of surface mechanical nano-crystallization to promote the nitriding process mainly includes the following: (1) The severe plastic deformation on the surface of the deformation-treated sample makes the refinement of the grains reach the nanometer level, which increases the grain boundary volume fraction and the density of defects such as dislocations, and provides more channels for the diffusion of nitrogen atoms. These active channels maintain good stability at higher temperatures. (2) The presence of high-density grain boundaries within the deformed nano-scale layer enhances the nitride nucleation rate. (3) The severe plastic deformation treatment increases the chemical activity of the surface, which promotes the chemical reaction during the nitriding process. (4) The severe deformation of the surface triggers the phase transition of the surface layer, which promotes the diffusion of nitrogen atoms [109–111].

However, in order to achieve the best performance of surface mechanical nano-crystallization to promote nitriding, the following issues need to be paid attention to [126]: (1) The surface roughness should not be too large, otherwise it will inhibit the nitriding process and cause poor surface integrity, which will affect the surface performance. (2) The surface mechanical nano-pretreatment process and the nitriding process need to achieve the best match. (3) According to the requirements of the service performance of the surface layer, the structure of the surface-composite-modified layer is reasonably designed, and the appropriate mechanical nano-technology method is selected to organically combine with the nitriding process.

3.2.3. Effect of Surface Mechanical Nano-Crystallization on Nitriding Efficiency

The effects of surface mechanical nano-crystallization on nitriding efficiency are compared and analyzed from the four aspects of nitriding time, nitriding temperature, structure of the nitrided layer, and hardness of the nitrided layer. According to the summary of the literature, the comparison histogram of the uniformity of surface nano-gas nitriding and conventional gas nitriding efficiency is obtained after taking the average values, as shown in Figure 9.

(1) Nitriding time: The pretreatment of surface mechanical nano-crystallization can shorten the nitriding time of gas nitriding to 70%. Sun et al. [127] performed mechanical grinding on the surface of pure iron and then carried out nitriding treatment in an ammonia atmosphere. It was found that the nitriding depth of the SMAT sample was greater than that of the untreated sample, and the nitriding time was also reduced by about 30%. Therefore, the nitriding time of gas nitriding can be shortened and the production efficiency can be improved through the pretreatment of surface mechanical nano-meterization.

(2) Nitriding temperature: The pretreatment of surface mechanical nano-crystallization can reduce the nitriding temperature of gas nitriding to 96%. The effect of SMAT on nitriding temperature is not clear. However, some studies have shown that surface mechanical nano-treatment can slightly reduce the nitriding temperature. Proust et al. [128] nano-sized the thin-grained layer on the surface of 316L stainless steel and found that the nitriding temperature of the sample after surface nano-treatment was lower than that of the untreated sample in the same atmosphere and the nitriding depth was also larger. However, other studies have shown that surface mechanical nano-treatment has no significant effect on

nitriding temperature. Tong et al. [129] nano-sized a thin crystal layer on the surface of pure iron and then carried out nitriding treatment under nitrogen atmosphere. It was found that the nitriding temperature of the sample after surface nano-treatment was not much different from that of the untreated sample. Taken together, SMAT has no significant effect on the nitriding temperature of gas nitriding.

(3) Nitrided layer structure: A better structure of the nitrided layer can be obtained through the pre-treatment of the surface mechanical nano-crystallization, and the grains are refined to 73%. Liu et al. [130] nano-sized a TiN film on the surface of Ti6Al4V alloy and found that the permeation layer of the sample after surface nano-treatment was denser and more uniform. In a study, untreated tool steel and tool steel with surface mechanical nano-treatment were subjected to gas nitriding treatment. The results showed that the grain size of the nitride layer treated with surface mechanical nano-treatment is about 30% lower than that without SMAT. Therefore, the pretreatment of SMAT can improve the gas nitrided layer structure and obtain a denser layer.

(4) Nitrided layer hardness: Surface mechanical nano-crystallization can increase the hardness of the gas-nitrided layer to 135%. The results of studies may be different due to the influence of surface mechanical nano-processing methods, processing time, processing conditions, and other factors. Generally, the hardness of materials treated with surface mechanical nano-technology can be increased by 10% to 50% compared with untreated materials. Yang et al. [74] performed ball milling and heat treatment on the surface of 40Cr steel and then carried out plasma nitriding under ammonia atmosphere. It was found that the hardness of the samples treated with surface nano-crystallization was higher than that of the untreated samples. It should be noted that although the surface mechanical nano-treatment can improve the hardness of the material, too high a hardness will also bring about problems such as brittleness. Therefore, the balance of factors such as hardness and toughness need to be considered comprehensively in practical applications.

3.3. Surface-Active Catalytic Nitriding

3.3.1. Accelerating Nitriding Mechanism of Surface-Active Catalytic Nitriding

Surface-active catalytic nitriding is a technology that uses surface catalysts to promote gas reactions on the surface of materials. Adding a surface-active infiltrating agent into the furnace by means of surface coating, dripping, and gas-solid mixing can reduce the activation energy of the workpiece surface during gas nitriding. It can also increase the decomposition rate of adsorbed ammonia on the workpiece surface, realize low-temperature gas nitriding, and improve nitriding efficiency [42,43]. During the gas nitriding process, surface-active catalysis nitriding can provide additional reaction sites and promote the adsorption and reaction of nitrogen molecules to accelerate the nitriding rate [131]. In addition, surface-active catalytic nitriding can realize the nitriding reaction at a lower temperature and reduce the influence of nitriding temperature on the material to improve the heat resistance and mechanical properties of the material [132]. Overall, surface-active catalysis is an effective gas nitriding technology that can achieve an efficient nitriding process at lower temperatures, resulting in improved material performance and durability.

According to the different types of elements, surface-active penetrating agents can be divided into two categories: One is the alloying elements (Me), mainly Ni, C, Ti, B, and other elements. The difference in N affinity between alloying elements and Fe is used to control the characteristics of the gas nitrided layer, thereby obtaining an excellent nitrided layer with thin compound layer; a thick, effective hardened layer; high hardness; and high toughness [133–135]. The other is rare-earth elements (Re). The characteristics of high chemical activity and large atomic radius (40% larger than iron) are used to increase the diffusion rate of the nitrogen atoms [136,137].

3.3.2. Effect of Surface-Active Catalytic on Nitriding Behavior

Effect of Alloying Elements (Ni, C, Ti, B, etc.) on Nitriding Behavior

During the gas nitriding process, the nitrogen atoms absorbed on the surface of the workpiece participate in the nitriding reaction and diffuse into the matrix, resulting in the development of the diffusion zone. In the nitrogen supply medium (nitriding atmosphere), iron can directly react with nitrogen, resulting in the formation of a layer of iron nitride on the surface of the sample at the top of the diffusion zone when the nitrogen potential is high enough. This layer of iron nitride is the so-called compound layer [138]. The active catalysis of alloying elements uses its affinity for nitrogen more strongly than for iron and preferentially interacts with nitrogen in the diffusion zone to regulate the phase characteristics of the nitrided layer and improve the performance of the nitrided layer [139]. The grain composition, crystal structure, and morphology of alloying elements (Me) and nitrides (MeN_x) have a significant effect on controlling the properties of iron-nitride-based components [140].

As shown in Equation (7), one mole of MeN_x develops from one mole of Me atoms initially dissolved in the nitrogen-free ferrite matrix lattice during the precipitation process. By comparing the molar volume of the nitride crystal (v_{MeN_x}) with that of the ferrite matrix crystal (v_{Fe}), it was found that the crystal structure of the nitrides may be incompatible with that of the ferrite matrix, resulting in the precipitation of non-equilibrium crystal structures or even amorphous metastable nitrides. And, the volume mismatch between the nitride precipitates and the ferrite matrix and the exposed crystal confinement at the precipitate/matrix interface can lead to strain [141].

$$\frac{\Delta v}{v} = \frac{v_{\text{MeN}_x} - v_{\text{Fe}}}{v_{\text{Fe}}} \times 100\% \quad (7)$$

The interaction strength of Me and N can be characterized by the chemical Gibbs energy (ΔG_{chem}), and the strain energy (ΔG_{strain}) generated during the precipitation process can significantly slow down the nitriding precipitation process. The interaction between chemical Gibbs energy (ΔG_{chem}) release and strain energy (ΔG_{strain}) consumption is shown in Equation (8) [142].

$$I = -\frac{\Delta G_{\text{chem}}}{\Delta G_{\text{strain}}} \quad (8)$$

The precipitation kinetics of nitrides are mainly affected by the development of misfit-strain fields and their relaxation rates caused by the coherent \rightarrow incoherent transition at the Me-nitride/ α -Fe interface [143,144]. It is now possible to precisely determine the various types of (excess) nitrogen present in the nitrided microstructure. Armed with this knowledge, physics-based models are being developed that can describe nitriding behavior.

Inia et al. [145] took the lead in preparing a 6–45 nm thick Ni coating on the surface of pure iron by electron beam evaporation or electrochemical deposition. Then low-temperature nitriding was carried out in a pure NH_3 medium at 325 °C for 45 min. The distribution of N elements in the obtained nitrided layer is shown in Figure 10. It was found that a large amount of iron oxide was formed on the surface of the pure iron without coating pretreatment, and the maximum concentration of N was only 5 wt.%. The N concentration of the nitriding pure iron pretreated with Ni coating is in the range of 20–30 wt.% and reaches the maximum when the concentration of O atoms is reduced to the minimum under the action of Ni coating. The active N produced by the decomposition of NH_3 diffuses into the Ni coating. Due to the different affinity of Ni and Fe for N, N desorbs on the surface of the Ni coating and diffuses through the Ni coating to the underlying substrate. This results in a sufficiently high nitrogen potential at the coating–substrate interface to form nitrides in iron or steel. During nitriding, the Ni coating provides part of the metal surface and satisfies the kinetic barrier for N uptake from NH_3 , which is lower than that of the iron oxide surface. These results indicate that the presence of Ni coating plays a role in promoting nitriding. Subsequently, the team prepared a nickel coating with a thickness of

about 36 nm on a surface of pure iron and carried out low-temperature nitriding in a pure NH_3 medium at a temperature lower than $300\text{ }^\circ\text{C}$ for 30 min to obtain a non-porous iron nitrided layer [146].

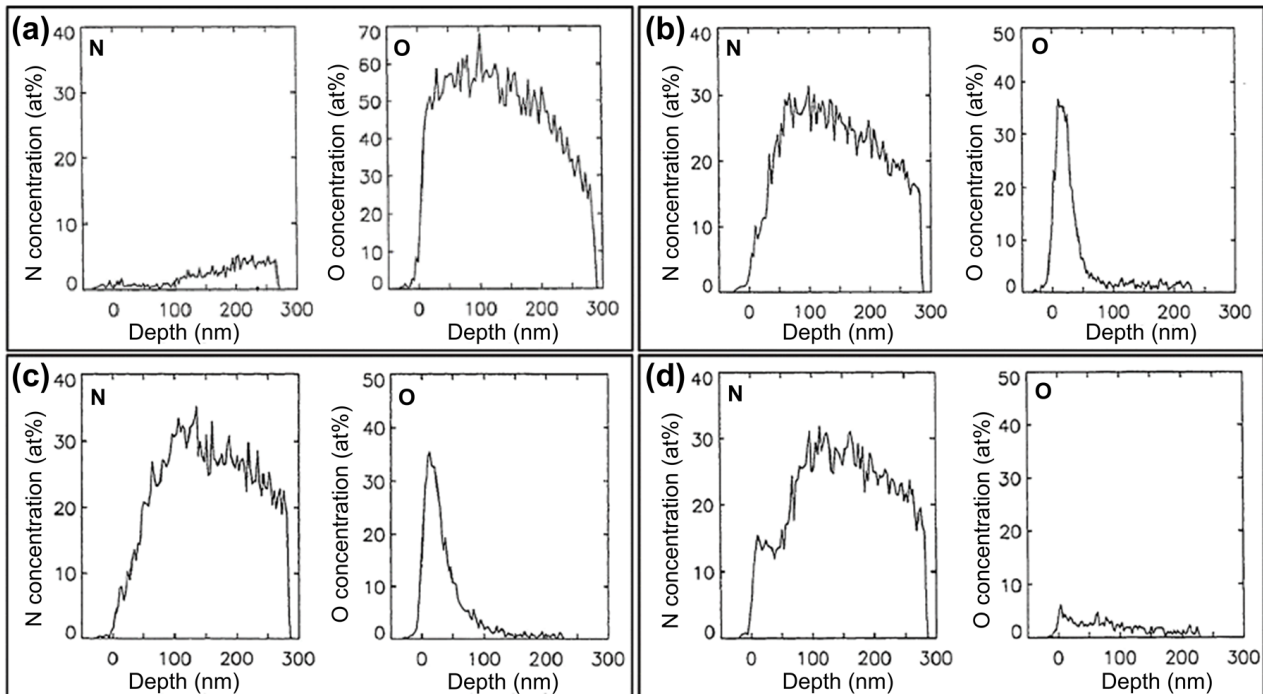


Figure 10. (a) Depth profiles of N and O after uncoated Fe and Fe covered with different thicknesses of Ni coating after nitriding in pure NH_3 at $325\text{ }^\circ\text{C}$ for 45 min, (b) 6 nm, (c) 25 nm, (d) 45 nm [146]. Adapted with permission from [146], copyright 1997 American Institute of Physics.

Steiner et al. [140] found that carbides were less stable than nitrides by comparing the Gibbs formation energies of carbides and nitrides. At 773 K ($500\text{ }^\circ\text{C}$), the Gibbs formation energy of Ti to TiN is -268 kJ/mol , and the Gibbs formation energy of Ti to TiC is -174 kJ/mol . During the nitriding process, the carbides generated due to the tempering treatment are dissolved, reprecipitated, or directly converted into nitrides. If a compound layer is formed on the surface of the sample, the carbon released by the nitride formation may infiltrate into the compound layer if the nitrogen potential in the surrounding atmosphere is sufficiently high. If the compound layer cannot be formed on the surface of the sample, the carbon will diffuse into the atmosphere. Especially at a greater depth from the surface of the compound layer, the carbon released by the formation of nitrides may lead to local supersaturation of carbon so that carbon is precipitated in the form of cementite Fe_3C . During the nitriding process, the macroscopic compressive stress parallel to the surface of the compound layer along the diffusion zone makes the cementite preferentially formed on the grain boundary.

As shown in Figure 11, Mao et al. [147] carried out an innovative nitriding treatment with the addition of trace amounts of Ti on 42CrMo steel. It was found that the addition of trace amounts of Ti can significantly improve the properties of the nitrided layer and obtain a high-hardness and high-toughness nitrided layer with less compound layer. It can also significantly increase the nitriding efficiency at the same time. Under the process condition of $540\text{ }^\circ\text{C} \times 4\text{ h}$, adding a trace amount of Ti can significantly increase the thickness of the effective hardened layer, from $225\text{ }\mu\text{m}$ in conventional nitriding to $380\text{ }\mu\text{m}$. The nitriding efficiency is increased by nearly 70%. When the thickness of the effective hardened layer is increased, the thickness of the compound layer is reduced from $19\text{ }\mu\text{m}$ in conventional nitriding to $10\text{ }\mu\text{m}$. The thickness of the compound layer is reduced by about 50%. The ratio of the compound layer to the effective hardened layer in the permeation layer is reduced from 8.5% to 2.6%. At the same time, a small amount of titanized layer was added

to form a high-hardness strengthening phase TiN, which increased the surface hardness of the nitrided layer from 703 HV_{0.05} to 895 HV_{0.05}. Adding a small amount of Ti has obtained excellent nitrided layer characteristics for the thin compound layer and the thick, effective hardened layer as well as high hardness and high toughness. The nitrided layer has important research and application value for improving impact resistance and wear resistance under the heavy load of ion nitrided parts.

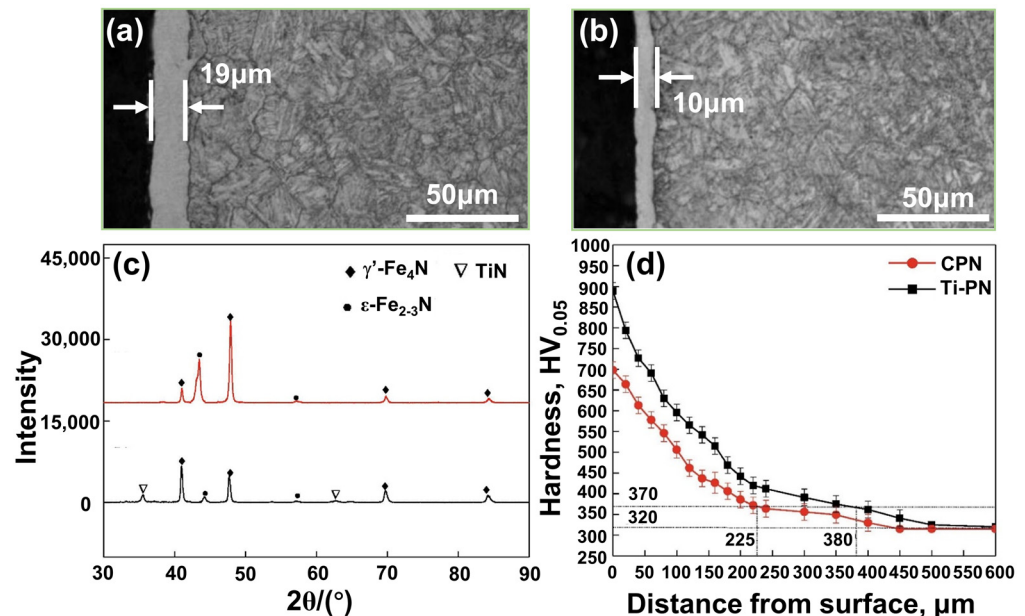


Figure 11. (a,b): Cross-sectional microstructure of samples treated by different processes for 42CrMo steel, (c) X-ray diffraction patterns of samples treated by different processes for 42CrMo steel, (d) cross-sectional microhardness profile of samples treated by different processes for 42CrMo steel [147]. Adapted with permission from [147], Copyright 2020 Elsevier.

Zheng et al. [148] used 42CrMo steel as the material to explore the effect of adding a small amount of B on the nitriding efficiency and the structure of the nitrided layer. The research results show that the addition of trace B can significantly improve the nitriding efficiency. Under the same nitriding process, the thickness of the compound layer increases gradually with the increase in B addition, from 18.78 μm to 29.44 μm. At the same time, ferron–boron compounds FeB and Fe₂B zigzag vertically wedged into the matrix and are formed at the junction of the compound layer and the diffusion layer, achieving the remarkable effect of enhancing the bonding force between the nitrided layer and the substrate and improving the hardness of the nitrided layer. With the increase in B addition, the surface hardness of the sample and the effective hardened layer depth are gradually increased, and the surface hardness can be increased from 750 HV_{0.05} to 1002 HV_{0.05}. The effective hardened layer thickness increased from 265 μm to 355 μm. The nitriding efficiency increased by about 35%.

All in all, the addition of alloying elements can improve the nitriding behavior of the material and improve properties such as penetration depth, hardness, and wear resistance. However, different alloying elements have different effects on the nitriding behavior, and excessive addition may lead to adverse effects. Therefore, it needs to be selected and optimized in specific applications.

Effect of Rare-Earth Elements (Re) on Nitriding Behavior

In the 1930s, B. Lehrer established the controllable nitriding phase diagram of nitriding temperature, nitrogen potential, and corresponding phase (as shown in Figure 4). From then on, the theoretical research and industrial application exploration of gas-controlled

nitriding began [87]. In the 1950s, the American Carpenter Company applied rare-earth elements to the treatment of stainless steel, and American steel foundries applied rare-earth elements to the surface treatment of metals. At the same time, researchers represented by Wei and Liu [149] introduced rare earths into the field of chemical heat treatment for the first time and made a major breakthrough in the rare-earth infiltration of steel, creating a precedent for rare-earth-catalyzed nitriding. In the 1980s, researchers at the Harbin Institute of Technology proposed the concept of rare-earth co-infiltration and gradually supplemented the theory of rare-earth-catalytic nitriding. In the late 1990s, scholars began to study the effect of rare earths on the surface modification behavior of plasma ion beam materials. In the 21st century, scientific researchers represented by Yan [150] have made remarkable achievements in the theory and application of rare-earth infiltration, which has promoted the practical engineering application of catalytic nitriding. After more than a century of continuous research and improvement, the theory and technology of rare-earth infiltration technology have been developed rapidly, and it has gradually become one of the most important chemical heat treatment processes. Table 1 shows the common rare-earth-catalyst processes and penetrants used in industrial production [151].

Table 1. Common rare-earth-catalyst processes and penetrants.

Process	Penetrant	Activator	Filler	Rare Earth
Monopermeable rare earth [152]	-	NH ₄ Cl, KCl	Al ₂ O ₃	Mixed ReCl, rare-earth metal nuggets (powder)
Rare-earth carburizing (Gas) [153]	Kerosene or natural gas	-	Methanol	ReCl, ReO, rare-earth powder
Rare-earth nitriding (Gas) [154]	Ammonia	-	Methanol	ReCl
Rare-earth boronizing [155]	B ₄ C, ferroboration	Al	SiC	ReCl, ReO, rare-earth powder
Rare-earth vanadium [156]	V ₂ O ₅	Al, Si	SiC	Misch metal
Rare-earth carbonitriding [157]	Carburization	Fluoride	Methanol	ReCl

In the nitriding process, N atoms always infiltrate along the tissue defects in the matrix first and then diffuse. The infiltration coefficient β and the diffusion coefficient D are commonly used to characterize the infiltration speed of nitrogen atoms. Nitriding temperature, nitrogen potential, material defect density, interfacial reactivity, and steel structure all affect these two parameters.

The effect of rare-earth-catalyzed nitriding is mainly reflected in two aspects: on the one hand, rare-earth atoms penetrate into steel, increasing the defect density inside the matrix, which increases the penetration coefficient β and diffusion coefficient D . However, conventional infiltration methods only increase the reactivity of the surface without increasing the defect density in the matrix, and the effect of infiltration is not ideal. On the other hand, the infiltration of rare-earth atoms is not evenly distributed. The scattered form cooperates with the Coriolis air mass to act simultaneously, which finally results in the uneven distribution of N atoms. Nitrogen atoms infiltrate to form nitrides with rare-earth as the core dispersed on the steel surface, and its shape changes from flake to quasi-spherical, which improves the infiltration effect [158]. The special electronic structure of rare-earth atoms can not only improve the nitriding efficiency but also improve the structure of the nitrided layer. Vein-like tissue is easily produced in the nitrided layer of conventional nitriding. The nitrides segregate along the grain boundaries, which increases the surface hardness and also increases the brittleness of the compound layer. Rare-earth-catalyzed nitriding distributes the nitrides with rare-earth atoms as the core in a diffuse and uneven distribution, which becomes a trap for interstitial nitrogen atoms. This will lead to the formation of a Coriolis air mass, effectively avoiding the segregation of nitrides along the grain boundaries and the generation of veins, improving the surface hardness and effectively reducing the brittleness of the compound layer [159]. Li et al. [160] found that

rare-earth-catalyzed nitriding of 12Cr1MoV steel increased the thickness of the nitrided layer, improved the strength and toughness of the compound layer, and improved the wear resistance of the nitrided layer. Torchane [161] found that the rare earths improved the diffusion kinetics of nitrogen atoms, increased the surface hardness and diffusion depth, and optimized the hardness gradient distribution through the gas nitriding of 32CrMoNiV5 steel with rare-earth elements.

Chen et al. [75] studied the effect of rare-earth additive La on the low-temperature gas nitriding of AISI 4140 steel. Before gas nitriding, a LaFeO_3 thin film was deposited on the surface of AISI 4140 using a LaFeO sol (gel precursor solution) by spin coating. Subsequently, gas nitriding treatment was carried out for 4 h under the conditions of 400, 475, and 550 °C when the flow rate of NH_3 was 5 L/min. It was found that LaFeO_3 is a typical ABO_3 rare-earth perovskite oxide, which has a good catalytic effect on gas nitriding. It effectively improves the thickness of the hardened layer and the microhardness, wear resistance, and corrosion resistance of the nitrided sample. As shown in Figure 12, the mechanism of action of LaFeO_3 catalytic coating can be divided into the following two aspects: (1) the equilibrium ratio between adsorbed N and dissolved N on the nitriding surface and (2) sufficient oxygen vacancies in LaFeO_3 provide more diffusion paths for N atoms. Subsequently, the same method was used to deposit LaFeO_3 film on the surface of 42CrMo steel, and it was verified again that LaFeO_3 can improve the efficiency of gas nitriding as a catalyst.

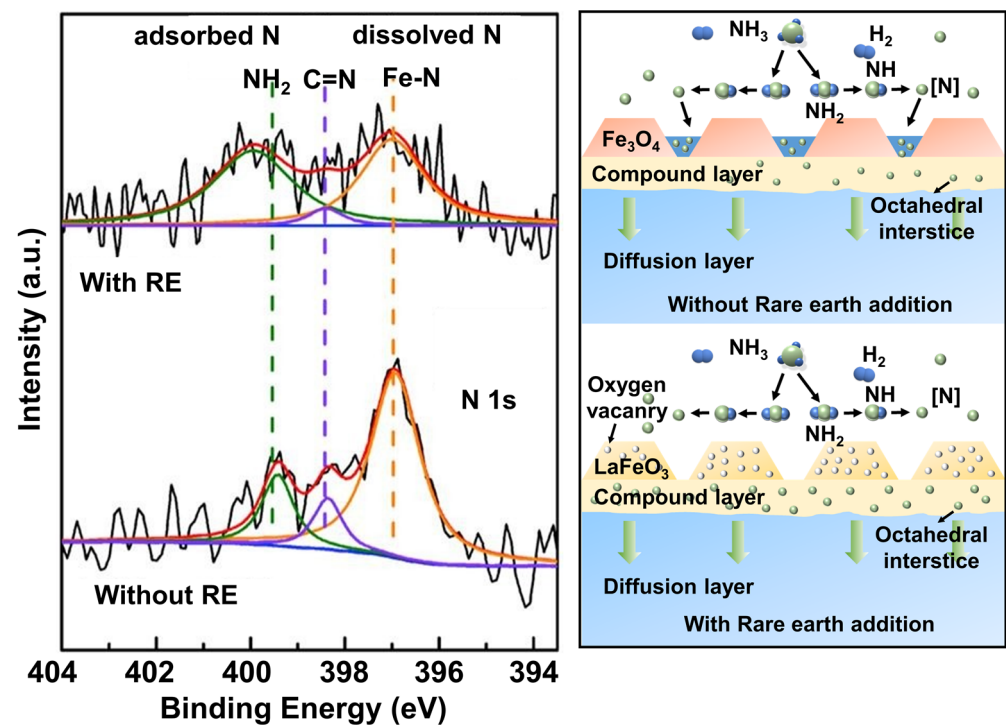


Figure 12. Mechanism of LaFeO_3 catalytic coating [75]. Adapted with permission from [75]; Copyright 2019 Elsevier.

Zhang et al. [131] used a chromium-, nickel-, and cerium-doped LaFeO_3 oxide coating to systematically study its effect on the catalytic nitriding efficiency of AISI 4140 steel. Its mechanism is shown in Figure 13. It was found that all ABO_3 oxides showed good catalytic activity in the low-pressure gas nitriding reaction, which mainly depended on the chemical state of the active oxygen on the surface of the sample. However, this state is affected by the valence state of the metal element being doped. With the extension of nitriding time, the catalytic activity of LaCrO_3 and LaNiO_3 oxides weakens, while that of LaFeO_3 and $(\text{La}_{0.5}\text{Ce}_{0.5})\text{FeO}_3$ oxides increases. When the ratio of adsorbed oxygen to hydroxyl on the

nitriding surface exceeds the critical value (1.33), ABO_3 oxide improves the efficiency of catalytic nitriding.

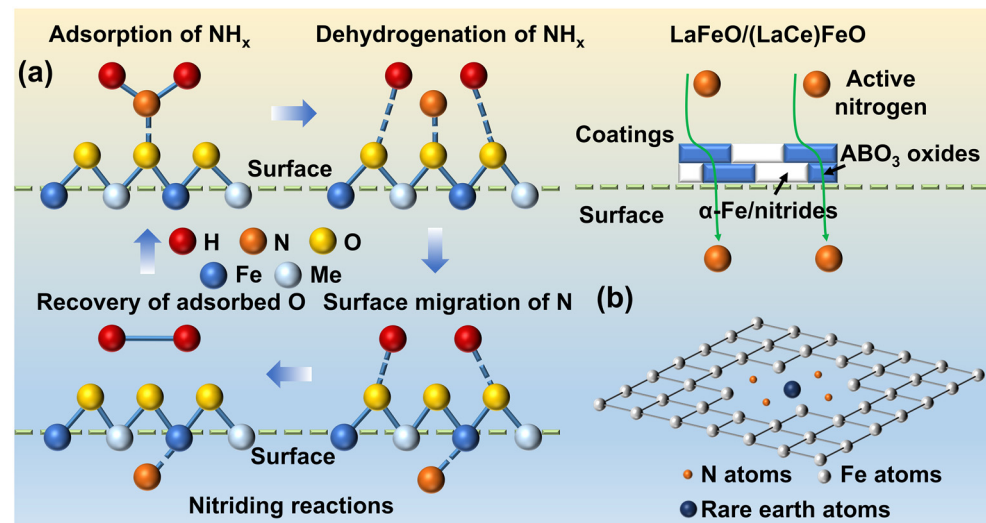


Figure 13. (a) Mechanism of ABO_3 oxide catalytic nitriding. (b) Distortion of rare-earth atoms infiltrated into Fe lattice.

In summary, improving the growth kinetics of the nitrided layer and reducing the surface activation energy of the nitrided workpiece are effective ways to improve the nitriding efficiency of the substrate material. During the nitriding process, we hope that the ammonia gas flowing through the surface of the nitriding workpiece will undergo thermal decomposition to generate active nitrogen atoms so that more active nitrogen atoms will be adsorbed and diffused into the metal substrate to achieve the purpose of improving nitriding efficiency. The use of surface-active penetrants can achieve this purpose. Adding the surface-active penetrants into the furnace through surface coating, dripping, and gas–solid mixing can reduce the activation energy of the workpiece surface during the gas nitriding process. It can increase the decomposition rate of adsorbed ammonia on the surface of workpiece and realize low-temperature gas nitriding, improving nitriding efficiency [140].

There are two types of surface-active penetrants. One is alloy elements (Me), mainly Ni, C, Ti, B, etc. The phase properties of the nitrided layer are adjusted by using the different affinity for N between alloying elements and Fe to obtain an excellent nitrided layer with a thin compound layer; a thick, effective hardened layer; high hardness; and high toughness. The other is rare-earth elements. The high chemical activity and large atomic radius of rare-earth elements are used to increase the diffusion rate of nitrogen atoms. However, in order to achieve the best performance of surface-active catalytic nitriding, the following issues need to be paid attention to: (1) Noble metals and rare-earth elements are used as ammonia decomposition catalysts. Although the catalytic activity is good, the cost is high. (2) Most studies on the application of surface-active catalytic coating pretreatment in nitriding of austenitic stainless steel still have the disadvantages of high nitriding temperature and long holding time. (3) The research on the performance and action mechanism of surface active penetrants on workpieces after nitriding is not adequate. (4) Past studies mainly focused on the nitriding behavior of binary Fe-based alloys, which should be applied to the nitriding process of multi-element Fe-based alloys.

3.3.3. Effect of Surface-Active Catalytic Nitriding on Nitriding Efficiency

The effects of surface-active catalytic nitriding on nitriding efficiency are compared and analyzed from the four aspects of the nitriding time, nitriding temperature, structure of nitrided layer, and hardness of nitrided layer. As shown in Figure 14, the efficiency

comparison histogram of surface-active catalytic nitriding and conventional gas nitriding is obtained after taking the average value according to the literature summary.

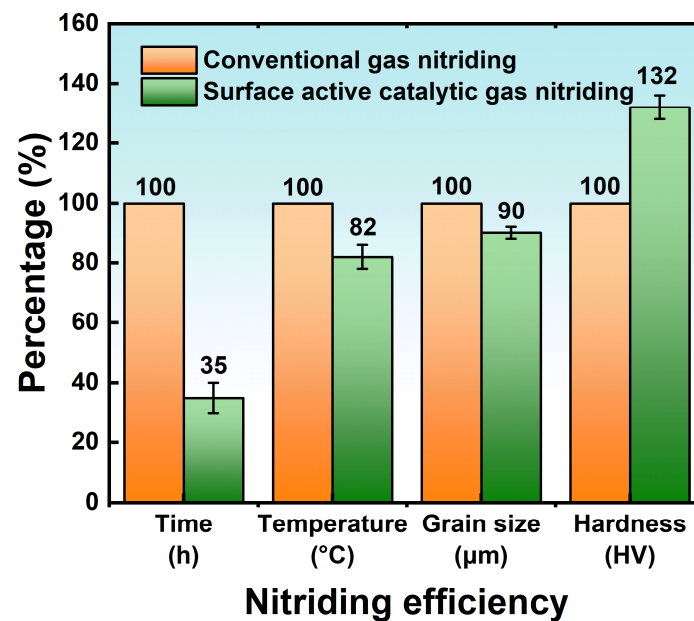


Figure 14. Histogram of efficiency comparison between surface-active catalytic nitriding and conventional gas nitriding.

(1) Nitriding time: Surface-active catalytic nitriding can shorten the time of gas nitriding by up to 35%. Taking the low-temperature gas nitriding promoted by surface-active catalytic nitriding as an example, the study [75,162] found that in the presence of a penetrant, the nitriding time can be shortened to about one-third to one-quarter. And, the hardness and wear resistance of the nitrided layer were also significantly improved. In contrast, the nitriding time takes longer to achieve the same thickness and hardness of the nitrided layer in the case of no penetrant. Therefore, surface-active catalytic nitriding can shorten the nitriding time and improve production efficiency.

(2) Nitriding temperature: Surface-active catalytic nitriding can reduce the temperature of gas nitriding to 82%. Surface-active catalytic nitriding can realize the nitriding reaction at a lower temperature, thereby reducing the influence of nitriding temperature on the material and improving the heat resistance and mechanical properties of the material. Yasuda et al. [163] found that in the presence of penetrant, the nitriding temperature can be reduced by more than 100 °C, and the hardness and wear resistance of the nitrided layer are comparable to those of traditional high-temperature nitriding. Therefore, surface-active catalytic nitriding can reduce the temperature of gas nitriding and promote the formation of the nitrided layer and improve its performance.

(3) Nitrided layer structure: Surface-active catalytic nitriding can obtain a better structure of the nitrided layer, and the grains are refined to 90%. Studies have shown that in the presence of penetrant, the structure of the nitrided layer can be transformed from the traditional structure of “inner-film middle layer/outer film” to a uniform single-layer structure. This structure can improve the compactness and bonding force of the nitrided layer to significantly improve the wear resistance and corrosion resistance of the material [131,164]. Therefore, the pretreatment of surface-active catalytic nitriding can improve the structure of the nitrided layer and obtain a denser layer.

(4) Nitrided layer hardness: Surface-active catalytic nitriding can increase the hardness of nitrided layers up to 132%. Studies have shown that in the presence of penetrant, the hardness after nitriding can be increased by about 20%–50% compared with traditional nitriding. At the same time, the penetrant can promote the uniform distribution of nitrogen, avoid the limitation of solid solubility of nitrogen in the nitriding process, and further

improve the hardness and wear resistance of the nitrided layer [43,165]. Therefore, higher hardness can be obtained by surface-active catalytic nitriding.

3.4. Surface Pre-Oxidized Nitriding

3.4.1. Accelerating Nitriding Mechanism of Surface Pre-Oxidized Nitriding

When the metal surface is treated by the method of pre-oxidation, a thin oxide film will be formed on the metal surface, and this oxide film is mainly composed of Fe_3O_4 and Fe_2O_3 . As shown in Figure 15, surface pre-oxidation will form a thin layer of dense oxide film on the surface of the workpiece, during which the following reactions occur [166]:

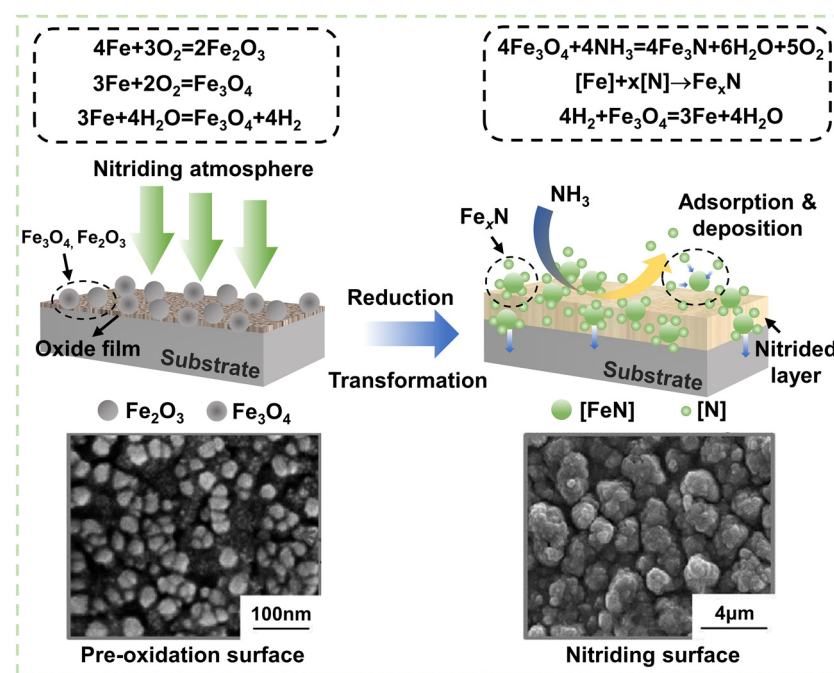
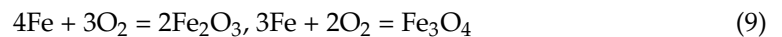


Figure 15. Schematic diagram of the mechanism of surface pre-oxidation catalytic nitriding [166]. Adapted with permission from [166], copyright 2019 Elsevier.

In the gas nitriding stage, under the reducing action of ammonia and hydrogen, the oxide film is continuously reduced and combined with active nitrogen atoms, enriched on the surface of the workpiece. And, because the oxide film is continuously reduced to form a loose and porous structure, the diffusion channel of nitrogen atoms is increased, and the chance of nitrogen atoms being adsorbed on the surface is increased [46]. The following reactions may occur:



It can be seen from Equations (9)–(13) that the oxide film is constantly replaced by nitride to increase the thickness of the effective nitrided layer and improve the nitriding efficiency.

There are three main methods of surface pre-oxidation: air pre-oxidation, anodic oxidation, and micro-arc oxidation technology [167,168].

The air pre-oxidation method places the workpiece in the air and heats it to 300–600 °C (usually 450–500 °C is the best), and the holding time is 30–90 min to oxidize the surface to form a thin oxide film. The air pre-oxidation method has the advantages of simple operation, low cost, and no need to add additional equipment, so it is suitable for promotion in industrial production [169].

The anodic oxidation method is the process of preparing an oxide film on the surface of the anode in the corresponding electrolyte under the action of an external current using electrode reaction and electric field drive to make metal particles and oxygen ions migrate directionally. At present, the research is mainly focused on the preparation of highly ordered anodized film and subsequent treatment process conditions, fine adjustment of anodized pore size and film thickness, and anodized film as a template to prepare various nano-tube materials. Relevant studies have proved that the oxide film structure prepared by the anodic oxidation method is a super penetrant in the nitriding process, and the effect is excellent [46].

The micro-arc oxidation method is developed from ordinary anodic oxidation. Its process is simpler than anodic oxidation, and its film characteristics are better than the anodic oxidation method. Micro-arc oxidation technology refers to placing the workpiece in the electrolyte and using the principles of plasma chemistry and electrochemistry to generate spark discharge on the surface of the material. The oxide film layer is prepared on the surface of metal materials through the joint action of electrochemistry, thermochemistry, and plasma chemistry [170,171].

The air pre-oxidation method, anodic oxidation method, and micro-arc oxidation method all have obvious catalytic effects in the process of material nitriding. Among them, the air pre-oxidation method is easy to operate and low cost and is suitable for popularization in production.

3.4.2. Effect of Surface Pre-Oxidation on Nitriding Behavior

Surface pre-oxidation can increase the diffusion rate of nitrogen atoms and promote the formation of nitrides. It can also improve the initial wear resistance, seizure resistance, and mechanical fatigue strength of the workpiece surface. After adopting the surface pre-oxidized nitriding, Zhang et al. [172] found that the thickness of the nitrated layer on the surface of the base material 42CrMo steel increased, and the thickness of the effective diffusion layer was significantly improved.

Under the same nitriding process, the thickness of the nitrated layer without surface pre-oxidation treatment is only 6.15 µm. However, the thickness of the nitrated layer after surface pre-oxidation treatment increased. And, when the pre-oxidation process is 300 °C × 30 min, the thickness of the nitrated layer reaches the maximum value of 15 µm. Li et al. [46,173] used the Owens–Wendt formula to calculate the surface free energy of 42CrMo steel treated with different pre-oxidation processes. The surface free energy calculation formula is as follows:

$$\gamma_s = \gamma_s^p + \gamma_s^d \quad (14)$$

where γ_s is the surface free energy, γ_s^p is the polar component of the surface free energy, and γ_s^d is the dispersive component of the surface free energy. The results show that when the pre-oxidation process is 300 °C × 30 min, the γ_s^p and γ_s^d are the largest. The surface free energy calculated by Formula (14) is the largest. The higher the surface free energy is, the more unstable the structure is, thus playing a significant role in promoting gas nitriding [167].

Ma [174] found that surface pre-oxidized nitriding improved the surface hardness of the base material 30Cr3Mo steel and increased the thickness of the nitrated layer. During the nitriding process, the formed ϵ phase is a key factor affecting the surface hardness of the nitrated layer. At the initial stage of nitriding, the active N atoms quickly formed alloy nitrides with high dispersion on the surface of the sample under the effect of infiltration. Two to three h after the start of surface pre-oxidized nitriding, the nitrated layer began to increase rapidly, and the hardness of the sample appeared at the highest value. Since the

formed high-hardness dispersed nitride hardly decomposes, the hardness of the sample is maintained until the end of nitriding. Compared with surface pre-oxidized nitriding, the dispersion of alloy nitrides formed on the surface of the sample by conventional nitriding is lower. This will result in a lower surface hardness after nitriding than the surface pre-oxidized nitriding. Under the same conditions of material, nitriding temperature, and NH_3 decomposition rate in the furnace, the nitriding speed mainly depends on the nitrogen absorption capacity of the surface of the sample. The use of surface pre-oxidized nitriding increases the probability and adsorption capacity of active N atoms on the surface of the sample, and enhances the nitrogen absorption capacity of the sample surface [175]. Moreover, a high concentration gradient is established on the surface of the sample at the initial stage of nitriding, which improves the diffusion activation energy of N atoms in the sample.

Wang [176] carried out surface pre-oxidized nitriding on the surface of 40Cr steel and found that the thickness of the nitrided layer increased. The hardness and wear resistance were also improved. A nitrided layer with a thickness of 24–39 μm is formed on the surface of the conventional nitriding sample, and the nitrided layer is mainly a white layer. The thickness of the nitrided layer on the surface of the pre-oxidized nitriding sample increases to 100–140 μm , and the nitrided layer is composed of a white layer and a gray layer. The nitrided layer is mainly composed of $\epsilon\text{-Fe}_3\text{N}$ and $\gamma'\text{-Fe}_4\text{N}$ phases. The white, light layer part is mainly ϵ phase, and the gray layer part is γ' phase [53]. In the wear test, compared with the conventional nitriding samples, the wear loss of the nitrided layer of the surface pre-oxidized nitriding samples is less. It can be concluded that as the thickness of the nitrided layer increases after pre-oxidation, the friction coefficient of the sample surface decreases, indicating that pre-oxidized nitriding improves the initial wear resistance of the sample surface.

In summary, the surface pre-oxidation treatment process has a significant catalytic effect on nitriding. The compound layer on the surface of the workpiece after surface pre-oxidation treatment is thicker than that of the conventional nitriding workpiece, and the thickness of the effective diffusion layer is significantly increased. After surface pre-oxidation, a large number of uniformly distributed nano-scale oxide particles are formed on the surface of the material, accompanied by microcracks and holes. And the surface free energy is the largest. These surface features are conducive to the adsorption of nitrogen and further diffusion to the substrate, thereby effectively increasing the nitriding rate. The microstructure of the nitrided layer on the surface of the surface pre-oxidized sample is mainly composed of $\epsilon\text{-Fe}_3\text{N}$ and $\gamma'\text{-Fe}_4\text{N}$ phases. The white, light layer part is mainly ϵ phase, and the gray layer part is γ' phase [53,88]. As the thickness of the nitrided layer increases after pre-oxidation, the friction coefficient of the sample surface tends to decrease, and the surface pre-oxidation improves the initial wear resistance of the sample surface.

However, the surface pre-oxidized nitriding has the following problems: (1) The surface corrosion resistance of the sample after pre-oxidation treatment cannot be completely improved, and it is easy to cause the decline of the surface corrosion resistance under some pre-oxidation processes. (2) The surface pre-oxidized nitriding is first the reduction process of the oxide layer on the surface of the workpiece. The nitriding can only be carried out after the oxide layer has been completely reduced. Nitriding total time = oxide layer reduction time + nitriding time. For the same pre-oxidation process, the reduction time of the oxide layer is certain. Therefore, reasonable control of the proportion of oxide layer reduction time in the entire process is the key to improving nitriding efficiency.

3.4.3. Effect of Surface Pre-Oxidation on Nitriding Efficiency

The effects of surface pre-oxidation on nitriding efficiency are compared and analyzed from the four aspects of the nitriding time, nitriding temperature, structure of the nitrided layer, and hardness of the nitrided layer. As shown in Figure 16, the efficiency comparison histogram of surface pre-oxidized nitriding and conventional gas nitriding is obtained after taking the average value according to the literature summary.

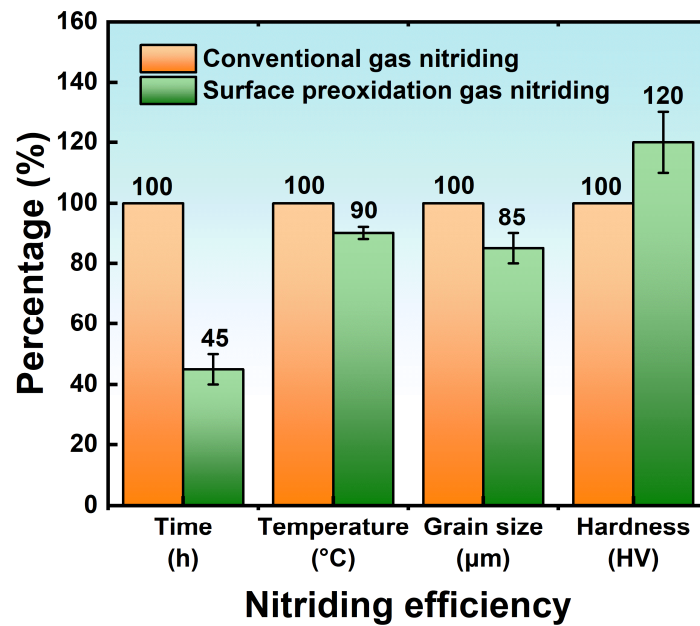


Figure 16. Histogram of efficiency comparison between surface pre-oxidized nitriding and conventional gas nitriding.

(1) Nitriding time: Surface pre-oxidation can shorten the nitriding time to 45%. The effect of surface pre-oxidation treatment on nitriding time mainly depends on factors such as material type, pre-oxidation conditions, and nitriding conditions. Taking titanium alloy as an example, the pre-oxidation treatment can shorten the nitriding time and improve the quality of the nitrated layer. Studies have shown that at 800 °C, titanium alloys pre-oxidized for 5 h can form a complete nitrated layer when the nitriding time is 5 h. However, titanium alloys without pre-oxidation treatment require more than 15 h of nitriding time to form a complete nitrated layer [177,178]. This indicates that pre-oxidation treatment can significantly shorten the nitriding time. Therefore, surface pre-oxidation can shorten the nitriding time of gas nitriding and improve production efficiency.

(2) Nitriding temperature: Surface pre-oxidation can reduce the nitriding temperature to 90%. The impact of surface pre-oxidation on nitriding temperature is mainly achieved by affecting the formation temperature and growth rate of the nitrated layer. Taking stainless steel as an example, oxidized stainless steel can form a dense and uniform nitrated layer at a lower temperature. For example, with ammonia gas as the nitriding source, at 540 °C, a dense Fe₄N layer can be formed on the surface of pre-oxidized stainless steel. However, stainless steel that has not been oxidized needs to be nitrated at a high temperature above 600 °C to form a similar nitrated layer [179,180]. Therefore, surface pre-oxidation can reduce the nitriding temperature, promote the formation of nitrated layer and improve its performance.

(3) Nitrated layer structure: Surface pre-oxidation can obtain better nitrated layer structure, with grain refinement to 85%. Surface pre-oxidation can reduce the number of holes and cracks in the nitrated layer and improve the compactness and smoothness of the nitrated layer, thereby improving the corrosion resistance, wear resistance, and fatigue life of the nitrated layer. For example, a study showed that plasma nitriding after pre-oxidation on the surface of stainless steel resulted in a denser and more uniform nitrated layer than pure nitriding. This improves the corrosion resistance, hardness, and wear properties of stainless steel [178]. Surface pre-oxidation can also affect the chemical composition and crystal structure of the nitrated layer. For example, studies have shown that nitriding after surface pre-oxidation can significantly reduce the nitrogen content in the nitrated layer while increasing the nitride grain size and solid solution element content in the nitrated layer, thus affecting the nitrated layer crystal structure and mechanical properties [181].

Therefore, surface pre-oxidation can improve the structure of nitrided layer and obtain a denser layer.

(4) Nitrided layer hardness: Surface pre-oxidation can increase the hardness of nitrided layer to 120%. Studies have shown that the hardness after surface pre-oxidized nitriding can be increased by about 20–50% compared with traditional nitriding [182]. Surface pre-oxidation can also promote the uniform distribution of nitrogen, avoid the solid solubility limit of nitrogen in the nitriding process, and further improve the hardness and wear resistance of the nitrided layer [183]. Therefore, the nitrided layer with higher hardness can be obtained by surface pre-oxidation.

3.5. Surface Laser Treatment

3.5.1. Accelerating Nitriding Mechanism of Surface Laser Treatment

Figure 17 shows the mechanism of surface laser treatment catalytic nitriding. Surface laser treatment concentrates the energy of the laser beam on the surface of the material to increase the temperature and cool it rapidly to form a certain depth of melting zone and heat-affected zone, thereby improving the surface properties of the material, such as wear resistance, corrosion resistance, and mechanical fatigue life [48]. In the process of surface laser treatment, the selection of parameters such as laser beam power, scanning speed, and scanning line distance can affect the depth and shape of the nitrided layer, thereby controlling the properties of the treated material. The main mechanism includes the following aspects [48–50]:

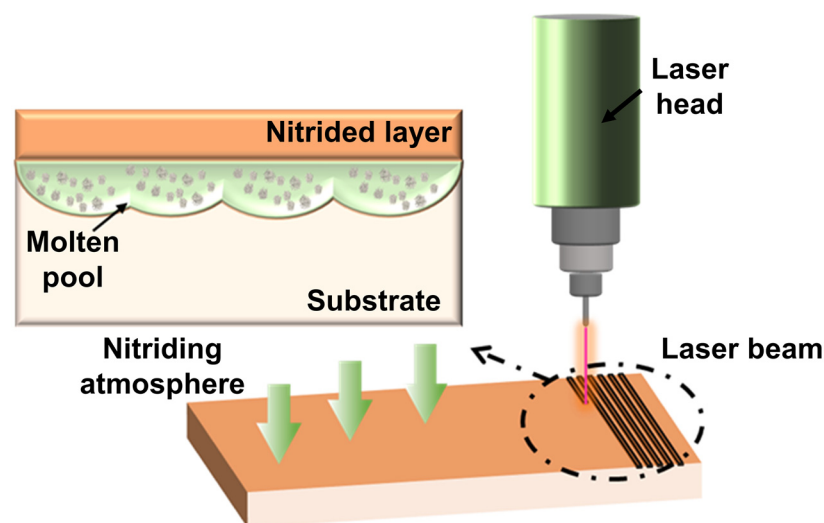


Figure 17. Schematic diagram of the mechanism of surface laser treatment catalytic nitriding.

Surface melting: When the laser beam concentrates its energy on the surface of the material, it creates a localized area of high temperature that melts the surface material. During the melting process, the oxides and impurities in the material are reduced and volatilized so that the surface of the material is purified and the purity is improved. Surface melting can promote the diffusion of nitrogen atoms and increase the nitriding rate. It can also improve the density and uniformity of the nitrided layer.

Rapid cooling: Under the effect of the laser beam, the molten material on the surface will rapidly cool and solidify, forming a certain depth of melting zone and heat-affected zone. Rapid cooling can lead to refinement and deformation of the lattice structure, which changes the physical properties of the material. Rapid cooling can effectively improve the hardness and wear resistance of the nitrided layer. However, if the cooling rate is too fast, it may cause cracks and brittleness in the nitrided layer.

Residual Stress: Residual stress is due to temperature gradients caused by the rapid heating and cooling of the surface during laser processing. After laser treatment, there is

residual stress between the nitrided layer formed on the surface and the substrate, which can improve the hardness and wear resistance of the nitrided layer. But, it may also cause peeling and cracking of the nitrided layer.

Spoilage reaction: Under the effect of the laser beam, chemical reactions may occur on the surface of the material, such as carbonization and nitriding, thereby changing the chemical composition of the material and improving the hardness and wear resistance. The spoilage reaction refers to the process in which nitrogen atoms diffuse into the substrate to form a solid solution or a metastable phase during laser processing. The modification reaction can increase the strength and toughness of the substrate, but it may also reduce the hardness and wear resistance of the nitrided layer.

During laser processing, fast heating and cooling rates will lead to the formation of a large number of defects such as dislocations, twins, and vacancies in the nitrided layer. This significantly speeds up the kinetic process of diffusion, lowers the energy barrier for nitride nucleation, and promotes the formation of nitrides [184,185]. Therefore, compared with other conventional methods, the surface laser treatment has unique advantages, such as fast speed, a small heat-affected zone, and avoiding unnecessary heating of the substrate. It also enables precise spatial and lateral processing of metal surfaces and adapts to materials with complex surface shapes [186]. The introduction of this surface laser treatment can significantly improve the surface hardness of the nitrided layer and optimize the hardness gradient distribution of the nitrided layer.

3.5.2. Effect of Surface Laser Treatment on Nitriding Behavior

Surface laser treatment has been widely used in surface modification of materials and preparation of penetrants. In terms of gas nitriding, surface laser treatment also significantly affects nitriding behavior, which is mainly reflected in the following three aspects [48,107]: (1) Adjustment of the surface microstructure of the material and improvement of the surface reactivity and surface energy, thereby promoting the nitriding reaction; (2) changing the composition and chemical state of the penetrant, thereby changing the stoichiometry of nitride formation; and (3) controlling nitride deposition location and morphology by adjusting surface structure and energy distribution.

Kulka et al. [27] found that surface laser treatment optimized the microstructure of the nitrided layer on the surface of the substrate material 42CrMo4 steel, improving wear resistance and hardness. As shown in Figure 18, a porous ϵ phase appeared on the surface of the sample, and a dense nitrided layer with $(\epsilon + \gamma')$ phase appeared below this region after surface laser treatment. The appearance of the γ' phase is mainly due to its precipitation from the ϵ nitrides during cooling. The entire surface compound layer is composed of white compound area and diffusion area, in which the diffusion area is composed of nitrate sorbite containing γ' nitride precipitates and a small part of martensite. The appearance of martensite improves the wear resistance and hardness of the sample.

Yan et al. [185] studied the effect of conventional gas nitriding (GN) and surface laser treatment (including laser surface melting and laser surface hardening) on the microstructure and properties of P20 steel. Figure 18 shows the microstructure of the upper surface area of all specimen cross-sections. As shown in Figure 18a, the microstructure of the original sample (OS) without gas nitriding treatment is mainly composed of coarse bainite. As shown in Figure 18b, the initial microstructure of the sample after conventional gas nitriding is still mainly composed of coarse bainite. As shown in Figure 18c,d, the coarse-grained martensite in the laser surface melting (LSM) sample has a larger aspect ratio compared with the laser surface hardening (LSH) sample. This is because the coarse columnar austenite grains in the LSM specimens are formed during the solidification of the surface melt layer, which facilitates the growth of martensite in the lateral direction. For the LSM sample, the denitriding effect of the molten metal reduces the nitrogen content of the surface layer, and the holes formed at the bottom of the molten layer destroy the continuity of the sample material and reduce the cooling rate of the surface material. Therefore, coarse-grained martensite is still formed on the surface of the LSM sample [187].

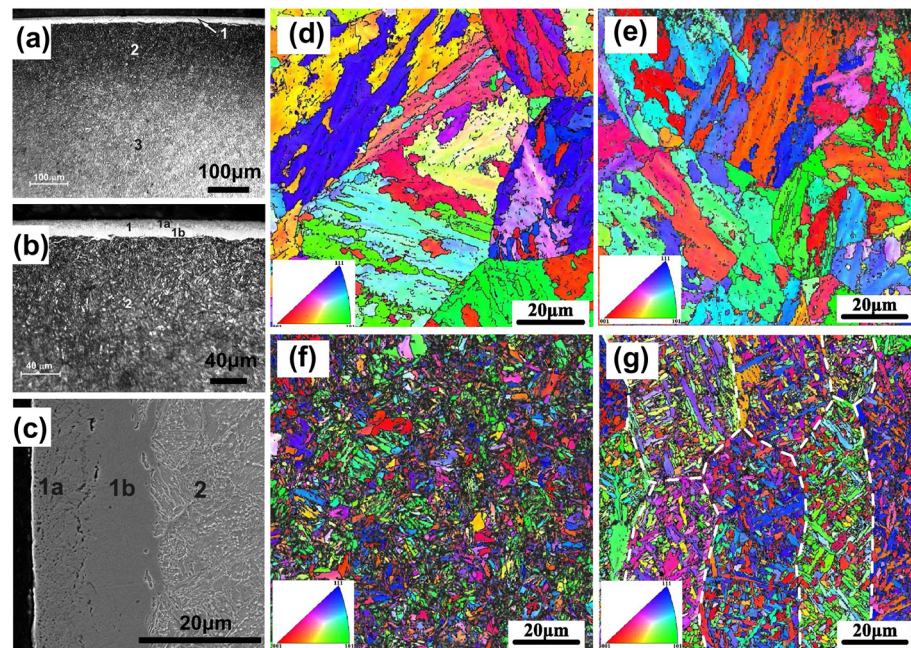


Figure 18. Microstructure of nitrided layer on the surface of 42CrMo4 steel [27]. (a,b) OM image. (c) SEM image: 1a, ϵ phase region; 1b, $\epsilon + \gamma'$ phase region; 2, diffusion zone. Microstructure of the upper surface area of the cross-section of the P20 steel sample [185]. (d) OS sample, (e) GN sample, (f) LSH sample, (g) LSM sample. Adapted with permission from [27], copyright 2016 by Elsevier. Adapted with permission from [185], copyright 2020 by Elsevier.

Surface laser treatment improves the hardness and wear resistance of the nitrided layer. This is due to the solid solution strengthening and Hall–Petch strengthening caused by the formation of martensite on the surface, which enhances the lattice deformation of α -Fe. It is beneficial for surface properties [188]. In addition, compared with conventional gas nitriding, the martensite grain size formed on the surface after surface laser treatment is smaller. Microstructure refinement also plays an important role in the improvement of surface hardness.

Zong et al. [189] carried out surface laser treatment catalytic nitriding on commercial pure titanium TA2 alloy and systematically analyzed the evolution mechanism of the nitrided layer by means of finite-element thermal field simulation and microstructure characterization. It was found that surface laser treatment increased the rate of formation of the nitrided layer. The microstructure of the nitrided layer formed TiN phase, α -Ti(N) phase, and $(\alpha + \alpha')$ phase sequentially from the surface to the center.

During the laser heating stage, the stable TiN phase and α -Ti(N) phase are formed with the increase in nitrogen solid solution. During the cooling phase, the α' phase (nitrogen-containing martensite) is formed ahead of the surrounding α phase. After laser surface nitriding treatment, since the N content gradually decreases from the substrate surface to the interior of the alloy, the α' martensite lath formed near the substrate surface is fine, while the α' martensite lath formed near the alloy interior is thick. And, it also has directional growth characteristics.

Zhang et al. [190] found that the surface hardness of TC4 alloy can reach 800 HV after surface laser treatment catalytic nitriding. Increasing the laser power increases the area of the melting zone, increases the number of TiN dendrites formed in the nitriding area on the surface of the TC4 alloy, and increases the thickness of the nitrided layer of the TiN layer.

In summary, the surface laser treatment can significantly improve the hardness and wear resistance of the nitrided layer. After the surface laser treatment, the deformation of the metal substrate is small, and the metallurgical bonding strength with the nitrided layer is high. The preparation cycle is short, the size of the workpiece is not limited, and the

material can be processed locally flexibly, with no pollution and no contact. The structure of the surface modification layer is controllable, and the excellent nitriding process is realized. However, the surface laser treatment has the following problems: (1) In the surface laser treatment catalytic nitriding process, the irradiation power density and scanning speed of the high-energy laser beam affect the performance of the nitrided layer. The greater the irradiation power density and scanning speed, the better the performance of the nitrided layer. But, in this case the energy loss is higher. (2) Although the nitriding process of surface laser treatment has been studied, the basic mechanism of the nitriding process, such as the migration of nitrogen outside the metal surface and the chemically active state of nitrogen gas, is still unclear due to the complexity and short time of the nitriding process.

3.5.3. Effect of Surface Laser Treatment on Nitriding Efficiency

The effects of surface laser treatment on nitriding efficiency are compared and analyzed from the four aspects of the nitriding time, nitriding temperature, nitrided layer structure, and nitrided layer hardness. As shown in Figure 19, the efficiency comparison histogram of surface laser treatment catalytic nitriding and conventional gas nitriding is obtained after taking the average value according to the literature summary.

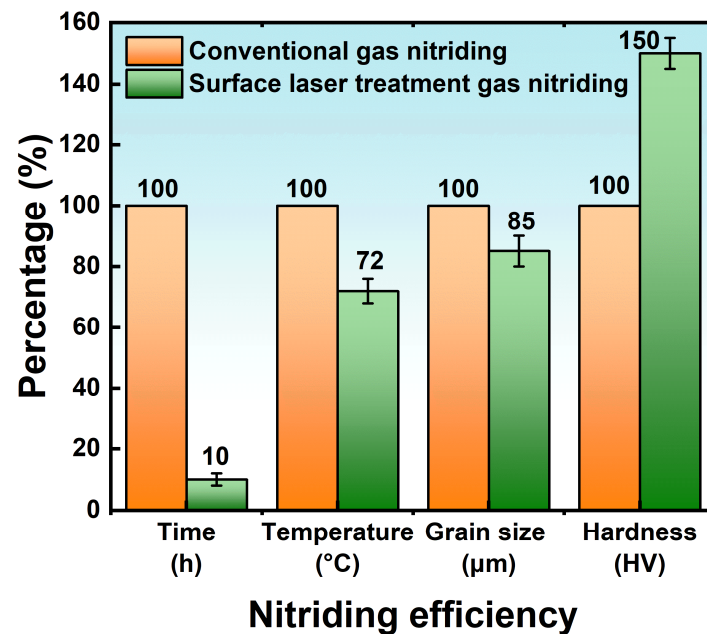


Figure 19. Histogram of efficiency comparison between surface laser treatment catalytic nitriding and conventional gas nitriding.

(1) Nitriding time: Surface laser treatment can shorten the nitriding time to 10%. Some studies have shown that using surface laser treatment method, nitriding in a shorter time (2 h) can form a nitrided layer with high hardness and excellent wear resistance [191]. Therefore, surface laser treatment can carry out gas nitriding in a short time and obtain a thinner but more uniform nitrided layer, shorten the nitriding time, and improve the production efficiency.

(2) Nitriding temperature: Surface laser treatment can reduce the nitriding temperature to 72%. Using surface laser treatment catalytic nitriding at lower temperature (400 °C), smaller grain size and higher hardness can be obtained [192]. Temperature also affects the grain growth and precipitate formation in the nitrided layer, thereby affecting the structure and properties of the nitrided layer [193]. Therefore, surface laser treatment can reduce the nitriding temperature, promote the formation of the nitrided layer, and improve its performance.

(3) Nitrided layer structure: Surface laser treatment can improve the structure of the nitrided layer, and the grains are refined to 85%. Surface laser treatment can promote the occurrence of nitriding reaction and improve the density and uniformity of the nitrided layer. Some studies have shown that surface laser treatment can inhibit the formation of pores and cracks in the nitrided layer and form a finer grain structure, improving the wear resistance and toughness of the nitrided layer [194]. Laser treatment can also change the type and number of precipitates in the nitrided layer, thereby adjusting the mechanical properties and chemical stability of the nitrided layer [195]. Therefore, surface laser treatment can improve the nitrided layer structure and obtain a denser layer.

(4) Nitrided layer hardness: Surface laser treatment can increase the hardness of the nitrided layer up to 150%. Some studies have shown that surface laser treatment can significantly increase the thickness and hardness of the nitrided layer and form a more uniform nitrided layer structure [196]. Surface laser treatment can also promote the formation of precipitates in the nitrided layer, which further increases hardness and wear resistance [197]. When the nitriding temperature is increased from 500 °C to 560 °C, the surface hardness increases by about 55%. However, when the nitriding time was increased from 4 h to 10 h, the surface hardness increased by about 50%. Therefore, higher hardness of the nitrided layer can be obtained by surface laser treatment.

4. Comparison of Technical Economy and Technology Readiness Level of Various Infiltration Methods

4.1. Technical Economy

Table 2 lists the comparison of energy consumption, cost, and CO₂ emission of different gas nitriding processes. In order to ensure the reliability and accuracy of the data, those studies with high factors, such as reliable data sources, abundant experimental data, reasonable experimental conditions, and sufficient sample size, were selected as references. The data in the table are obtained by calculation. The formulas for calculating energy consumption, cost, and CO₂ emissions are explained in detail below:

(1) Energy consumption calculation formula [198].

$$\text{Energy consumption} = \text{Total power of nitriding equipment} \times \text{Nitriding time.}$$

where the total power of nitriding equipment includes heating power, nitrogen flow power, and ammonia flow power. When calculating, the power and time are calculated according to the reactor size, heating method, temperature, gas flow, and other parameters of different processes. The calculation is converted to the standard unit, the kilowatt-hour (kWh).

(2) Cost Calculation Formula [199].

Cost calculation includes investment cost and operating cost. Total cost = CAPEX + OPEX.

Investment cost refers to the cost of building a new factory or updating equipment, including equipment procurement, construction costs, transportation costs, etc. Adopt the index CAPEX (capital expenditure) calculation method. CAPEX = construction cost/equipment capacity. Operating costs refer to daily operating costs, including electricity, gas, maintenance, etc. Adopt the index OPEX (operating expenditure) calculation method. OPEX = operating expenses/production capacity.

Calculate CAPEX and OPEX according to the reactor size, heating method, temperature, gas flow, and other parameters of different processes. Convert the calculation result to the standard unit, the United States dollar (USD). The unit price and quantity of equipment refer to relevant literature and market conditions, and the annual operating time and cost are also obtained through literature and market research.

(3) CO₂ Emission Calculation Formula [200].

CO₂ emission = energy consumption of nitriding equipment × CO₂ emission coefficient. Nitriding equipment energy consumption refers to the energy consumed by the equipment during operation, such as electricity, natural gas, etc. The CO₂ emission coefficient refers to the CO₂ emission produced by unit energy consumption, and its value

depends on the type of energy. CO₂ emissions refer to the amount of carbon dioxide produced in the process; we use the carbon footprint calculation method. That is, CO₂ emissions = energy consumption × carbon dioxide emission factor. We refer to the carbon dioxide emission factor published by the International Energy Agency (IEA) and convert the calculation result into a standard unit, the kilogram (kg).

For the calculation of the values in the tables, average values have been assumed where there are ranges and numerical differences in various documents. References are cited for each value reported. No references were collected from the references mentioned in the last column of the table against their values. We emphasize that the numerical values reported here are indicative and wish readers to exercise caution when considering their application. In addition, readers are advised to develop their own methods based on the data presented here and the references cited. Here are some thoughts we made based on the data in the table:

The first is energy consumption. In the process of gas nitriding, a large amount of energy is consumed. Among them, gas nitriding (optimization of process parameters) under high-temperature and high-pressure conditions requires a large amount of electric energy or fuel, which is currently one of the most common gas nitriding methods. For example, in industrial production, it is usually necessary to use high-temperature and high-pressure ammonia gas for nitriding, which consumes a large amount of electric energy or fuel. Using other methods can significantly reduce energy consumption. The energy consumption of surface laser treatment is the lowest [17]. This is because surface laser treatment has the characteristics of short action time and obvious effect. This will greatly reduce the time and temperature required for nitriding, thereby reducing the energy consumption.

The second is carbon dioxide emissions. High energy consumption means high CO₂ emissions. Therefore, carbon dioxide emissions are directly proportional to energy consumption. From this perspective, energy-intensive optimization of process parameters and surface mechanical nano-crystallization may lead to higher CO₂ emissions. Therefore, for some environmentally friendly enterprises, these methods may not be the first choice. The energy consumption of surface pre-oxidation and surface laser treatment is relatively low, so their CO₂ emissions are also relatively low. It should be pointed out that the CO₂ emissions may vary depending on the application scenarios and actual operation methods.

For example, during the operation of process parameter optimization and surface mechanical nano-crystallization, it may be possible to choose to use some environmentally friendly energy sources to reduce carbon dioxide emissions [120,201]. Therefore, when conducting technical economy analysis, it is necessary to conduct detailed analysis of specific operation methods and application scenarios, and to conduct accurate calculation and evaluation of emissions.

Finally, there is the cost. The total cost is composed of investment cost and operating cost. The investment cost is the cost of purchasing, installing, and debugging equipment during the nitriding process and also includes the cost of labor, training, and qualification certification. Operating costs are the costs of maintaining and operating equipment during the nitriding process, including energy, materials, maintenance, labor, and other management costs [202]. It can be seen from the table that surface-active catalytic nitriding, surface pre-oxidized nitriding, and surface laser treatment require relatively high investment costs. The investment costs for process parameter optimization and surface mechanical nano-crystallization are relatively low. This is due to the limitations of the current technical level, the equipment required for surface pre-oxidized nitriding and surface laser treatment is relatively high-end, and the operation and maintenance of equipment also require high-end talents. In comparison, less equipment is required for process parameter optimization and surface mechanical nano-crystallization. Because of its relatively mature technology, it requires less investment [203].

Table 2. Comparison of energy consumption, cost, and CO₂ emission of different gas nitriding processes.

Type	Energy Consumption (kWh/kg)	CO ₂ Emissions (kg)	Indicative CAPEX (USD/year)	Indicative OPEX (USD/year)	Ref.
Conventional gas nitriding	35–45	6.5–7.5	300–350	40–45	[34,48,107,137]
Process parameter optimization	45–50	7.5–8.0	250–300	30–35	[22,71,98,100]
Surface mechanical nano-crystallization	15–20	4.5–5.5	450–500	55–60	[32,41,96,102]
Surface-active catalytic nitriding	12–15	3.5–4.5	750–800	70–75	[53,62,64,158]
Surface pre-oxidation	10–12	3–4	850–900	90–95	[75,127,169,180]
Surface laser treatment	8–10	2.5–3.5	1100–1150	100–105	[24,184,195,196]

4.2. Technology Readiness Level

TRL is a technology readiness-level assessment method proposed by the National Aeronautics and Space Administration (NASA) in the 1980s, which is used to describe the evolution process of a technology from laboratory research to practical application [204].

As shown in Table 3, the TRL rating system is usually divided into nine grades. The TRL scale is primarily aimed at the development and testing of engineered components, from Level 1 (initial generation of an idea) to Level 9 (daily use of the component in the operating environment for which it was designed). Levels 1 to 3 are generally referred to as basic research (proof of concept). Levels 4 to 6 are the development of components under increasingly realistic conditions (proof of principle). Levels 7 to 9 are components fully deployed in their designed (proof of performance) system through operational testing [205].

Table 3. Summary of TRL definition for gas nitriding process (adapted from ref. [205–207]).

TRL	Function	Definition
1–2	Proof of concept	Basic research is carried out in the laboratory, and further experimental verification and improvement are still needed.
3–4	-	Technical verification and prototype development are carried out in the laboratory, and further engineering verification is still required.
5–6	Proof of principle	Engineering verification and field demonstrations in laboratories and factories have reached a certain level of maturity, but further expansion and improvement are still needed.
7–8	-	Large-scale application and verification in the actual production environment has achieved practical application results.
9	Proof of performance	It has been widely used and achieved commercial success.

This article refers to a large number of studies and patents, mainly related to the research and practical experience of different gas nitriding processes and also combined with relevant industry standards and technical guidelines [208–216]. Table 4 presents the technology readiness level, reference project status, and CO₂ emission reduction potential of different gas nitriding processes.

Table 4. Technology readiness level, reference project status, and CO₂ mitigation potential of different gas nitriding process (adapted from refs. [208–216]).

Process	Technology Readiness Level	Reference Project Status and R&D	CO ₂ Emission Reduction Potential	Commercial Application	Ref.
Conventional gas nitriding	8	-	5	8	[192,210]
Process parameter optimization	7	-	3	7	[211,212]
Surface mechanical nano-crystallization	6	Researchers at the KTH Royal Institute of Technology in Stockholm, Sweden, are investigating the use of nano-processing to improve the nitriding process.	6	5	[213,214]
Surface-active catalytic nitriding	5	Researchers at the University of Duisburg-Essen in Germany are studying the use of transition metals, such as molybdenum, tungsten, and chromium, as catalysts to promote nitriding reactions.	7	4	[131,213]
Surface pre-oxidized nitriding	5	Researchers at the University of Surrey in the UK are investigating the use of oxidation pretreatments to improve the nitriding process.	4	3	[181,215]
Surface laser treatment	3	Researchers at the Swiss Federal Institute of Technology in Zurich are investigating the use of laser processing to improve the nitriding process.	8	2	[103,216]

According to the research and development stage, application field, and market acceptance of different processes, the TRL analysis of the five gas nitriding pretreatment methods, namely process parameter optimization, surface mechanical nano-crystallization, surface-active catalytic nitriding, surface pre-oxidized nitriding, and surface laser treatment, was carried out. The CO₂ emission reduction potential of different nitriding processes was analyzed from the aspects of energy saving, emission reduction, resource utilization, and environmental protection. The commercial application scoring criteria are the commercial application prospects and market competitiveness of different nitriding processes, including market size, competition status, industry trends, etc. It should be noted that the scoring standards and evaluation methods are only for reference, and comprehensive consideration and trade-offs need to be made in combination with specific situations in actual application. Different process schemes may have different advantages and disadvantages in different application scenarios, which need to be selected and adjusted according to the actual situation.

Combined with the data in the table, we analyze the TRL of the five methods one by one [205,209]:

Process parameter optimization: This method has a high TRL and has been widely used in industrial production. This method does not need to develop new equipment or processes but only needs to optimize existing equipment and processes, so the technology readiness level is relatively high.

Surface mechanical nano-crystallization: This method has a high TRL. It has been extensively studied and applied in actual production. With the continuous development of nano-technology, this method will be more widely used.

Surface-active catalytic nitriding: The TRL of this method is low and requires further research and development. Although some studies have shown that the addition of penetrants can improve the nitriding efficiency and the quality of the nitrided layer, further research is needed on the selection of penetrants, the amount of addition, and the mechanism.

Surface pre-oxidized nitriding: The TRL of this method is low and requires further research and development. Although some studies have shown that pre-oxidation can improve the nitriding efficiency and the quality of the nitrided layer, further research is needed on the thickness, composition, and influence of the oxidized layer on the properties of the material.

Surface laser treatment: This method has a low TRL and requires further research and development. Although some studies have shown that laser treatment can quickly obtain a high-quality nitrided layer, further research is needed on the mechanism of laser treatment, the stability and reliability of the equipment, and so on.

From the perspective of TRL, the technology readiness level of process parameter optimization and surface mechanical nano-crystallization is relatively high. The technology readiness level of surface-active catalytic nitriding, surface pre-oxidized nitriding, and surface laser treatment is relatively low, and further research and development are needed.

5. Conclusions and Future Work

As the global demand for renewable energy increases, the development of the wind power industry will continue to expand, and gas nitriding will become an integral part of the wind power industry. However, the treatment temperature of traditional gas nitriding is high, and the nitriding rate is slow, which is not in line with the current concept of double carbon development. Based on this, this review analyzes the research progress of conventional gas nitriding and summarizes the effect of catalytic methods on the behavior and efficiency of gas nitriding. Common gas nitriding and accelerating methods include optimizing process parameters (pressure and temperature), surface mechanical nano-crystallization, surface-active catalytic nitriding, surface pre-oxidized nitriding, and surface laser treatment.

Optimizing process parameters is one of the most commonly used methods in gas nitriding. By adjusting the pressure and temperature of gas nitriding, the nitriding depth and nitriding rate can be controlled. However, optimizing process parameters requires precise control of temperature and pressure and may result in surface oxidation or chemical reactions that reduce the efficiency.

Surface mechanical nano-crystallization is another common accelerating method, which can improve the efficiency of gas nitriding by reducing the surface roughness. This method can increase the nitriding depth and nitriding rate without changing the chemical composition of the sample but requires the use of complex nano-fabrication techniques and may affect the mechanical properties of the sample.

Surface-active catalytic nitriding is a method of accelerating gas nitriding using surface-active penetrants. By coating the surface of the part with a penetrant, the nitriding temperature can be lowered and the nitriding rate and depth can be increased. However, penetrants may cause surface chemical reactions or degrade the mechanical properties of the part.

Surface pre-oxidation is a method of surface oxidation treatment before gas nitriding. It reduces the occurrence of surface chemical reactions and increases the efficiency of gas permeation. However, surface pre-oxidation requires the use of special oxidation treatments and may lead to peeling or destruction of the oxide layer.

Surface laser treatment changes the chemical and physical properties of the surface by laser irradiation, thereby improving the efficiency of gas penetration. This method can increase the nitriding depth and rate without changing the chemical composition of the sample but requires the use of high-power lasers and may affect the mechanical properties of the sample.

In addition, these methods also have different defects in terms of energy consumption, carbon dioxide emissions, and technical maturity. In terms of energy consumption, the gas nitriding process requires a large amount of energy. For example, gas nitriding under the conditions of high temperature and high pressure requires a lot of electricity or fuel. Therefore, it is necessary to explore gas nitriding penetrants and catalytic methods with low energy consumption. In terms of CO₂ emissions, high energy consumption means

high CO₂ emissions. Therefore, it is necessary to develop a gas nitriding method with low energy consumption and low carbon dioxide emission to reduce the impact on the environment. In terms of technology readiness level, different methods have different degrees. For example, optimizing process parameters is one of the most commonly used gas nitriding methods, and the technology readiness level is relatively high. However, methods such as surface mechanical nano-crystallization and surface laser treatment are relatively new and require more experimental verification and optimization. Therefore, it is necessary to comprehensively consider factors such as energy consumption, carbon dioxide emissions, and technology readiness level when selecting a gas nitriding and accelerating method and to strive to develop a more environmentally friendly, low-energy gas nitriding method.

Aiming at these problems, it may be a good solution to use multiple techniques for collaborative preprocessing. By combining different pretreatment methods, their advantages can be maximized, thereby improving the efficiency and environmental protection of gas nitriding. This also needs to be formulated according to the specific situation to ensure the maximization of comprehensive benefits. For example, the method of synergistic pretreatment of surface mechanical nano-crystallization and surface-active catalytic nitriding can be considered. Surface mechanical nano-crystallization can improve the surface quality and micro-morphology through micro-grinding or impact treatment, thereby improving the efficiency of gas nitriding. Surface-active catalytic nitriding can increase the reaction rate by introducing a penetrant on the surface or adding a penetrant during the gas nitriding process, thereby further improving the efficiency of gas nitriding. This method can simultaneously solve the problems of surface quality and reaction rate, thereby improving the comprehensive benefits of gas nitriding. In addition, the method of synergistic pretreatment of surface mechanical nano-crystallization and surface pre-oxidation can also be considered. Surface pre-oxidized nitriding can improve the quality and thickness of the surface oxide layer through oxidation treatment, thereby increasing the reaction sites of gas nitriding and increasing the reaction rate. This method can solve the problem of surface quality and reaction sites to improve the efficiency of gas nitriding. It should be noted that for different materials and application scenarios, different preprocessing methods may produce different effects. When selecting and combining pretreatment methods, it is necessary to consider the characteristics of the material and the specific application requirements to develop the best solution.

In summary, different gas nitriding methods have their advantages and disadvantages. Choosing an appropriate method requires comprehensive consideration of component materials, surface topography, and nitriding depth. Using the synergistic effect of multiple pretreatment methods can improve the efficiency and reliability of gas nitriding. It is of great value and significance for industry development, double carbon implementation, and green and sustainable development. It is one of the important directions for the development of gas nitriding technology in the future.

Author Contributions: The manuscript was written through contributions of all authors. All authors have given approval to the final version of the manuscript.

Funding: Financial support from the National Science Foundation of China (Grant Nos. 52071032) and the Postgraduate Research & Practice Innovation Program of Jiangsu Province (KYCX23_3034 and SJCX23_1569).

Institutional Review Board Statement: Not applicable.

Informed Consent Statement: Not applicable.

Data Availability Statement: Not applicable.

Conflicts of Interest: The authors declare no conflict of interest.

References

1. Mendoza, J.M.F.; Ibarra, D. Technology-enabled circular business models for the hybridisation of wind farms: Integrated wind and solar energy, power-to-gas and power-to-liquid systems. *Sustain. Prod. Consum.* **2023**, *36*, 308–327. [\[CrossRef\]](#)
2. Watson, S.; Moro, A.; Reis, V.; Baniotopoulos, C.; Barth, S.; Bartoli, G.; Bauer, F.; Boelman, E.; Bosse, D.; Cherubini, A.; et al. Future emerging technologies in the wind power sector: A European perspective. *Renew. Sustain. Energy Rev.* **2019**, *113*, 109270. [\[CrossRef\]](#)
3. Lin, Z.; Liu, X. Wind power forecasting of an offshore wind turbine based on high-frequency SCADA data and deep learning neural network. *Energy* **2020**, *201*, 117693. [\[CrossRef\]](#)
4. Bharani, R.; Sivaprakasam, A. A meteorological data set and wind power density from selective locations of Tamil Nadu, India: Implication for installation of wind turbines. *Total Environ. Res. Themes* **2022**, *3–4*, 100017. [\[CrossRef\]](#)
5. Wang, H.; Lamichhane, T.N.; Paranthaman, M.P. Review of additive manufacturing of permanent magnets for electrical machines: A prospective on wind turbine. *Mater. Today Phys.* **2022**, *24*, 100675. [\[CrossRef\]](#)
6. Pogrenjak, A.D.; Bratushka, S.N.; Bersnev, V.M.; Levintant-Zayonts, N. Shape memory effect and superelasticity of titanium nickelide alloys implanted with high ion doses. *Russ. Chem. Rev.* **2013**, *82*, 1135–1159. [\[CrossRef\]](#)
7. Qian, H.; Chen, S.; Wang, T.; Cheng, G.; Chen, X.; Xu, Z.W.; Zeng, Q.; Liu, Y.; Yan, D.M. Silicon nitride modified enamel coatings enable high thermal shock and corrosion resistances for steel protection. *Surf. Coat. Technol.* **2021**, *421*, 127474. [\[CrossRef\]](#)
8. Zhang, J.; Wang, H. Development of offshore wind power and foundation technology for offshore wind turbines in China. *Ocean Eng.* **2022**, *266*, 113256. [\[CrossRef\]](#)
9. Dhanola, A.; Garg, H.C. Tribological challenges and advancements in wind turbine bearings: A review. *Eng. Fail. Anal.* **2020**, *118*, 104885. [\[CrossRef\]](#)
10. Nassar, N.T.; Wilburn, D.R.; Goonan, T.G. Byproduct metal requirements for US wind and solar photovoltaic electricity generation up to the year 2040 under various Clean Power Plan scenarios. *Appl. Energy* **2016**, *183*, 1209–1226. [\[CrossRef\]](#)
11. Vallejo, J.P.; Álvarez-Regueiro, E.; Cabaleiro, D.; Fernandez-Seara, J.; Fernandez, J.; Lugo, L. Functionalized graphene nanoplatelet nanofluids based on a commercial industrial antifreeze for the thermal performance enhancement of wind turbines. *Appl. Therm. Eng.* **2019**, *152*, 113–125. [\[CrossRef\]](#)
12. Yan, F.Y.; Chen, B.F.; Yao, J.W.; Zhang, D.L.; Yan, M.F.; Zhang, Y.X. Characterization of microstructure and corrosion properties of AZ91D magnesium alloy surface-treated by coating-nitriding. *J. Mater. Res. Technol.* **2021**, *14*, 1559–1568. [\[CrossRef\]](#)
13. Pohreliuk, I.M.; Yaskiv, O.I.; Fedirko, V.M.; Diuh, I.V. Effect of nitriding on the electrochemical behaviour of Ti-Al-Mn alloy. *Mater. Corros.* **2005**, *56*, 697–700. [\[CrossRef\]](#)
14. Zhang, Z.L.; Bell, T. Structure and corrosion resistance of plasma nitrided stainless steel. *Surf. Eng.* **1985**, *1*, 131–136. [\[CrossRef\]](#)
15. Peng, D.Q.; Kim, T.H.; Chung, J.H.; Park, J.K. Development of nitride-layer of AISI 304 austenitic stainless steel during high-temperature ammonia gas-nitriding. *Appl. Surf. Sci.* **2010**, *256*, 7522–7529. [\[CrossRef\]](#)
16. Dong, H. S-phase surface engineering of Fe-Cr, Co-Cr and Ni-Cr alloys. *Int. Mater. Rev.* **2010**, *55*, 65–98. [\[CrossRef\]](#)
17. Michalski, J.; Wach, P.; Tacikowski, J.; Betiuk, M.; Burdyski, K.; Kowalski, S.; Nakonieczny, A. Contemporary industrial application of nitriding and its modifications. *Mater. Manuf. Process.* **2009**, *24*, 855–858. [\[CrossRef\]](#)
18. Almeida, E.A.S.; Costa, C.E.; Milan, J.C.G. Study of the nitrided layer obtained by different nitriding methods. *Matéria* **2015**, *20*, 460–465. [\[CrossRef\]](#)
19. Tong, W.P.; Liu, C.Z.; Wang, W.; Tao, N.R.; Wang, Z.B.; Zuo, L.; He, J.C. Gaseous nitriding of iron with a nanostructured surface layer. *Scr. Mater.* **2007**, *57*, 533–536. [\[CrossRef\]](#)
20. Wang, B.; Fu, W.T.; Dong, F.; Jin, G.F.; Feng, W.W.; Wang, Z.H.; Sun, S.H. Significant acceleration of nitriding kinetics in pure iron by pressurized gas treatment. *Mater. Des.* **2015**, *85*, 91–96. [\[CrossRef\]](#)
21. Keddani, M.; Djeghlal, M.E.; Barrallier, L. A diffusion model for simulation of bilayer growth (ϵ/γ') of nitrided pure iron. *Mater. Sci. Eng.* **2004**, *378*, 475–478. [\[CrossRef\]](#)
22. Alekseeva, M.S.; Gress, M.A.; Scherbakov, S.P.; Gerasimov, S.A.; Kuksenova, L.I. The influence of high-pressure gas nitriding on the properties of martensitic steels. *Met. Sci. Heat Treat.* **2017**, *59*, 524–528. [\[CrossRef\]](#)
23. Singh, S.K.; Naveen, C.; Sai, Y.V.; Satish, U.; Bandhavi, C.; Subbiah, R. Experimental study on wear resistance of AISI 347 treated with salt bath nitriding and gas nitriding processes—a review. *Mater. Today Proc.* **2019**, *18*, 2717–2722. [\[CrossRef\]](#)
24. Kim, Y.H.; Kim, H.G. Effect of Gas Nitriding Characteristics on the Mechanical Properties after Pre-Heat Treatment of Stainless Steels. *J. Korean Soc. Heat Treat.* **2010**, *23*, 142–149.
25. Boztepe, E.; Alves, A.C.; Ariza, E.; Rocha, L.A.; Cansever, N.; Toptan, F. A comparative investigation of the corrosion and tribocorrosion behaviour of nitrocarburized, gas nitrided, fluidized-bed nitrided, and plasma nitrided plastic mould steel. *Surf. Coat. Technol.* **2018**, *334*, 116–123. [\[CrossRef\]](#)
26. Ichii, K. Structure of the ion-nitrided layer of 18-8 stainless steel. *Technol. Rep. Kansai Univ.* **1986**, *27*, 135.
27. Kundalkar, D.; Mavalankar, M.; Tewari, A. Effect of gas nitriding on the thermal fatigue behavior of martensitic chromium hot-work tool steel. *Mater. Sci. Eng.* **2016**, *651*, 391–398. [\[CrossRef\]](#)
28. Pellizzari, M.; Molinari, A.; Straffellini, G. Thermal fatigue resistance of gas and plasma nitrided 41CrAlMo7 steel. *Mater. Sci. Eng.* **2003**, *352*, 186–194. [\[CrossRef\]](#)
29. Akhtar, S.S.; Arif, A.F.M.; Yilbas, B.S. Evaluation of gas nitriding process with in-process variation of nitriding potential for AISI H13 tool steel. *Int. J. Adv. Manuf. Technol.* **2010**, *47*, 687–698. [\[CrossRef\]](#)

30. Moradshahi, M.; Tavakoli, T.; Amiri, S.; Shayeganmehr, S. Plasma nitriding of Al alloys by DC glow discharge. *Surf. Coat. Technol.* **2006**, *201*, 567–574. [[CrossRef](#)]
31. Funch, C.V.; Christiansen, T.L.; Somers, M.A.J. Gaseous nitriding of additively manufactured maraging steel; nitriding kinetics and microstructure evolution. *Surf. Coat. Technol.* **2022**, *432*, 128055. [[CrossRef](#)]
32. Li, G.M.; Liang, Y.L.; Sun, H.; Cao, Y.G. Nitriding behavior and mechanical properties of carburizing and nitriding duplex treated M50NiL steel. *Surf. Coat. Technol.* **2020**, *384*, 125315. [[CrossRef](#)]
33. Baranowska, J.; Arnold, B. Corrosion resistance of nitrided layers on austenitic steel. *Surf. Coat. Technol.* **2006**, *200*, 6623–6628. [[CrossRef](#)]
34. Somers, M.A.J.; Mittemeijer, E.J. Layer-growth kinetics on gaseous nitriding of pure iron: Evaluation of diffusion coefficients for nitrogen in iron nitrides. *Metall. Mater. Trans. A* **1995**, *26*, 57–74. [[CrossRef](#)]
35. Yang, S.; Yang, D.; Shi, W.; Deng, C.; Chen, C.; Feng, S. Global evaluation of carbon neutrality and peak carbon dioxide emissions: Current challenges and future outlook. *Environ. Sci. Pollut. Res.* **2023**, *30*, 81725–81744. [[CrossRef](#)] [[PubMed](#)]
36. Karakan, M.; Alsaran, A.; Celik, A. Effect of process time on structural and tribological properties of ferritic plasma nitrocarburized AISI 4140 steel. *Mater. Des.* **2004**, *25*, 349–353. [[CrossRef](#)]
37. Michalski, J.; Tacikowski, J.; Wach, P.; Ratajski, J. Controlled gas nitriding of 40HM and 38HMJ steel grades with the formation of nitrided cases with and without the surface compound layer, composed of iron nitrides. *Probl. Eksploat.* **2006**, *2*, 43–52.
38. Fattah, M.; Mahboubi, F. Comparison of ferritic and austenitic plasma nitriding and nitrocarburizing behavior of AISI 4140 low alloy steel. *Mater. Des.* **2010**, *31*, 3915–3921. [[CrossRef](#)]
39. Kumar, S.A.; Raman, S.G.S.; Narayanan, T.S.N.S.; Gnanamoorthy, R. Influence of counterbody material on fretting wear behaviour of surface mechanical attrition treated Ti–6Al–4V. *Tribol. Int.* **2013**, *57*, 107–114. [[CrossRef](#)]
40. Liu, B.; Wang, B.; Yang, X.D.; Zhao, X.F.; Qin, M.; Gu, J.F. Thermal fatigue evaluation of AISI H13 steels surface modified by gas nitriding with pre-and post-shot peening. *Appl. Surf. Sci.* **2019**, *483*, 45–51. [[CrossRef](#)]
41. Liu, J.; Suslov, S.; Vellore, A.; Ren, Z.C.; Amanov, A.; Pyun, Y.S.; Martini, A.; Dong, Y.L.; Ye, C. Surface nanocrystallization by ultrasonic nano-crystal surface modification and its effect on gas nitriding of Ti6Al4V alloy. *Mater. Sci. Eng.* **2018**, *736*, 335–343. [[CrossRef](#)]
42. Rodrigues, J.; Miranda, S.M.C.; Santos, N.F.; Neves, A.J.; Alves, E.; Lorenz, K.; Monteiro, T. Rare earth co-doping nitride layers for visible light. *Mater. Chem. Phys.* **2012**, *134*, 716–720. [[CrossRef](#)]
43. Zhang, C.; Wang, Y.; Chen, X.; Chen, H.T.; Wu, Y.Q.; Wang, Y.X.; Tang, L.N.; Cui, G.D.; Chen, D.Z. Catalytic behavior of LaFeO₃ perovskite oxide during low-pressure gas nitriding. *Appl. Surf. Sci.* **2020**, *506*, 145045. [[CrossRef](#)]
44. Zhang, C.S.; Yan, M.F.; Sun, Z. Experimental and theoretical study on interaction between lanthanum and nitrogen during plasma rare earth nitriding. *Appl. Surf. Sci.* **2013**, *287*, 381–388. [[CrossRef](#)]
45. Sueyoshi, H.; Hamaishi, K.; Kadomatsu, S.; Shiomizu, T.; Ohzono, Y. Effect of preheating in air on gas nitriding of SUS304. *Nippon Kinzoku Gakkaishi (1952)* **1996**, *60*, 616–623.
46. Lutz, J.; Mändl, S. Effect of ion energy and chemistry on layer growth processes during nitriding of CoCr alloys. *Nucl. Instrum. Methods Phys. Res. Sect. B* **2009**, *267*, 1522–1525. [[CrossRef](#)]
47. Li, S.X.; Chen, L.; Wang, M.T.; Yan, Z.Q. Effect of pre-oxidation and rare earth cerium on plasma nitriding of 42CrMo steel. *Heat Treat. Met.* **2021**, *46*, 186–189.
48. Schaaf, P. Laser nitriding of metals. *Prog. Mater. Sci.* **2002**, *47*, 1–161. [[CrossRef](#)]
49. Chen, X.K.; Wu, G.; Wang, R.; Guo, W.T.; Yang, J.P.; Cao, S.Z.; Wang, Y.L.; Han, W.H. Laser nitriding of titanium alloy in the atmosphere environment. *Surf. Coat. Technol.* **2007**, *201*, 4843–4846. [[CrossRef](#)]
50. Razavi, R.S.; Gordani, G.R.; Man, H.C. A review of the corrosion of laser nitrided Ti-6Al-4V. *Anti-Corros. Methods Mater.* **2011**, *58*, 140–154. [[CrossRef](#)]
51. Fang, B.Z.; Daniel, L.; Bonakdarpour, A.; Wilkinson, D.P. Upgrading the State-of-the-Art Electrocatalysts for Proton Exchange Membrane Fuel Cell Applications. *Adv. Mater. Interfaces* **2022**, *9*, 2200349. [[CrossRef](#)]
52. Zhao, M.M.; Huang, X.L.; Zhuang, D.M.; Sheng, L.; Xie, X.; Cao, M.; Pan, J.J.; Fan, H.Y.; He, J.P. Constructing porous nanosphere structure current collector by nitriding for lithium metal batteries. *J. Energy Storage* **2022**, *47*, 103665. [[CrossRef](#)]
53. Arabczyk, W.; Skulmowska, K.; Pelka, R.; Lendzion-Bielun, Z. Oscillatory Mechanism of α -Fe (N) \leftrightarrow γ' -Fe₄N Phase Transformations during Nanocrystalline Iron Nitriding. *Materials* **2022**, *15*, 1006. [[CrossRef](#)]
54. Sun, J.Q.; Wang, D.R.; Yang, J.; Li, F.J.; Zuo, L.L.; Ge, F.; Chen, Y.B. In Situ Preparation of Nano-Cu/Microalloyed Gradient Coating with Improved Antifriction Properties. *Coatings* **2022**, *12*, 1336. [[CrossRef](#)]
55. Wang, Y.; Lu, S.; Zheng, J.; Liang, L. Advances in Latest Application Status, Challenges, and Future Development Direction of Electrospinning Technology in the Biomedical. *J. Nanomater.* **2022**, *2022*, 3791908. [[CrossRef](#)]
56. Xu, W.C.; Cui, Z.D.; Zhu, S.L. Recent Advances in Open-Cell Porous Metal Materials for Electrocatalytic and Biomedical Applications. *Acta Metall. Sin.* **2022**, *58*, 1527–1544.
57. Bell, T. *Source Book on Nitriding*; American Society for Metals: Metals Park, OH, USA, 1977.
58. García Caballero, F.; Wang Fu, M.; Gao, M.C. *Encyclopedia of Materials: Metals and Alloys*; Elsevier: Amsterdam, The Netherlands, 2022.
59. Chen, W.L.; Wu, C.L.; Liu, Z.R.; Ni, S.; Hong, Y.; Zhang, Y.; Chen, J.H. Phase transformations in the nitrocarburizing surface of carbon steels revisited by microstructure and property characterizations. *Acta Mater.* **2013**, *61*, 3963–3972. [[CrossRef](#)]

60. Wu, C.L.; Tian, L.; Hong, Y.; Wang, J.; Chen, X.Y. The effect of cooling methods and subsequent ageing on the nitrided layer of pure-iron by gas nitriding at 580 °C. *J. Hunan Univ.* **2015**, *42*, 33–39.
61. Wu, C.L.; Luo, C.P.; Zou, G.F. Phase Transformations During Composite-Chromization of steel 20. *Acta Metall. Sin.* **2004**, *40*, 1074–1078.
62. Lin, Y.H.; Bohn, A.; Cheng, J.Y.; Handt, A.V.D.; Mara, N.A.; Poerschke, D. Gas nitriding behavior of refractory metals and implications for multi-principal element alloy design. *J. Alloys Compd.* **2023**, *947*, 169568. [[CrossRef](#)]
63. Xie, Y.; Miyamoto, G.; Furuhashi, T. High-throughput investigation of Cr-N cluster formation in Fe-35Ni-Cr system during low-temperature nitriding. *Acta Mater.* **2023**, *253*, 118921. [[CrossRef](#)]
64. Fare, S.; Lecis, N.; Brescia, E.; Mazzola, M. Role of grain boundaries in diffusional phenomena during gas nitriding of pure iron. *Procedia Eng.* **2011**, *10*, 2943–2948. [[CrossRef](#)]
65. Dupuis, R.D. Epitaxial growth of III–V nitride semiconductors by metalorganic chemical vapor deposition. *J. Cryst. Growth* **1997**, *178*, 56–73. [[CrossRef](#)]
66. Jiang, X.J.; Wang, S.Z.; Feng, Z.H.; Qi, H.B.; Fu, H.; Liu, R.P. Improving vacuum gas nitriding of a Ti-based alloy via surface solid phase transformation. *Vacuum* **2022**, *197*, 110860. [[CrossRef](#)]
67. Wang, J.; Shu, R.; Chai, J.L.; Rao, S.G.; Febvrier, A.L.; Wu, H.C.; Zhu, Y.B.; Yao, C.F.; Luo, L.H.; Li, W.P.; et al. Xe-ion-irradiation-induced structural transitions and elemental diffusion in high-entropy alloy and nitride thin-film multilayers. *Mater. Des.* **2022**, *219*, 110749. [[CrossRef](#)]
68. Dosssett, J.L.; Totten, G.E. Introduction to steel heat treatment. *Steel Heat Treat. Fundam. Process.* **2013**, *4*, 3–25.
69. Bell, T.; Mao, K.; Sun, Y. Surface engineering design: Modelling surface engineering systems for improved tribological performance. *Surf. Coat. Technol.* **1998**, *108*, 360–368. [[CrossRef](#)]
70. Gao, H.; Lysevych, M.; Tan, H.H.; Jagadish, C.; Zou, J. The effect of Sn addition on GaAs nanowire grown by vapor–liquid–solid growth mechanism. *Nanotechnology* **2018**, *29*, 465601. [[CrossRef](#)]
71. Wang, B.; Sun, S.H.; Guo, M.W.; Jin, G.F.; Zhou, Z.A.; Fu, W.T. Study on pressurized gas nitriding characteristics for steel 38CrMoAlA. *Surf. Coat. Technol.* **2015**, *279*, 60–64. [[CrossRef](#)]
72. Zhao, H.; Duan, L.; Chen, G.; Fan, H.Y.; Wang, J.; Zhou, C.C. High corrosion resistance performance of 304 stainless steel after liquid nitrocarburization. *Compos. Part B* **2018**, *155*, 173–177. [[CrossRef](#)]
73. Mirjani, M.; Mazrooei, J.; Karimzadeh, N.; Ashrafizadeh, F. Investigation of the effects of time and temperature of oxidation on corrosion behavior of plasma nitrided AISI 4140 steel. *Surf. Coat. Technol.* **2012**, *206*, 4389–4393. [[CrossRef](#)]
74. Li, Y.; Wang, L.; Zhang, D.D.; Shen, L. The effect of surface nanocrystallization on plasma nitriding behaviour of AISI 4140 steel. *Appl. Surf. Sci.* **2010**, *257*, 979–984. [[CrossRef](#)]
75. Chen, X.; Bao, X.Y.; Xiao, Y.; Zhang, C.S.; Tang, L.N.; Yao, L.; Cui, G.D.; Yang, Y. Low-temperature gas nitriding of AISI 4140 steel accelerated by LaFeO₃ perovskite oxide. *Appl. Surf. Sci.* **2019**, *466*, 989–999. [[CrossRef](#)]
76. Wang, L.; Zhou, W.L.; Shen, C.; Zhang, Y.L.; Li, F.; Ding, Y.H.; Xin, J.W.; Wang, B.S.; Hua, X.M. Effect of substrate temperature on microstructure and mechanical properties of TiAl alloy fabricated using the twin-wire plasma arc additive manufacturing system. *J. Mater. Sci.* **2022**, *57*, 8940–8955. [[CrossRef](#)]
77. Borgioli, F.; Galvanetto, E.; Fossati, A.; Bacci, T. Glow-discharge nitriding and post-oxidising treatments of AISI H11 steel. *Surf. Coat. Technol.* **2003**, *162*, 61–66. [[CrossRef](#)]
78. Xiang, J.; Han, Y.F.; Le, J.W.; Huang, G.F.; Xiao, L.; Liu, J.Y.; Lu, W.J. Effect of temperature on microstructure and mechanical properties of ECAPed (TiB+La₂O₃)/Ti-6Al-4V composites. *Mater. Charact.* **2018**, *146*, 149–158. [[CrossRef](#)]
79. Miyamoto, J.; Abbramo, P. The effect of plasma nitriding treatment time on the tribological properties of the AISI H13 tool steel. *Surf. Coat. Technol.* **2019**, *375*, 15–21. [[CrossRef](#)]
80. Wang, J.; Lin, Y.H.; Yan, J.; Zen, D.Z.; Zhang, Q.A.; Huang, R.B.; Fan, H.Y. Influence of time on the microstructure of AISI 321 austenitic stainless steel in salt bath nitriding. *Surf. Coat. Technol.* **2012**, *206*, 3399–3404. [[CrossRef](#)]
81. Arabczyk, W.; Zamlyny, J. Study of the ammonia decomposition over iron catalysts. *Catal. Lett.* **1999**, *60*, 167–171. [[CrossRef](#)]
82. Wołowicz-Korecka, E.; Michalski, J.; Kucharska, B. Kinetic aspects of low-pressure nitriding process. *Vacuum* **2018**, *155*, 292–299. [[CrossRef](#)]
83. Michalski, J.; Burdyński, K.; Wach, P.; Latas, Z. Nitrogen availability of nitriding atmosphere in controlled gas nitriding processes. *Arch. Metall. Mater.* **2015**, *60*, 747–754. [[CrossRef](#)]
84. Abboud, J.H.; Fidel, A.F.; Benyounis, K.Y. Surface nitriding of Ti-6Al-4V alloy with a high power CO₂ laser. *Opt. Laser Technol.* **2008**, *40*, 405–414. [[CrossRef](#)]
85. Michalski, J.; Wołowicz-Korecka, E. A study of parameters of nitriding processes. Part 1. *Met. Sci. Heat Treat.* **2019**, *61*, 183–190. [[CrossRef](#)]
86. Mitsui, H.; Kurihana, S. Solution nitriding treatment of Fe–Cr alloys under pressurized nitrogen gas. *ISIJ Int.* **2007**, *47*, 479–485. [[CrossRef](#)]
87. Lehrer, E. Über das Eisen-Wasserstoff-Ammoniak-Gleichgewicht. *Z. Elektrochem. Angew. Phys. Chem.* **1930**, *36*, 383–392.
88. Michalski, J.; Tacikowski, J.; Wach, P.; Lunarska, E.; Baum, H. Formation of single-phase layer of γ' -nitride in controlled gas nitriding. *Met. Sci. Heat Treat.* **2005**, *47*, 516–519. [[CrossRef](#)]
89. Nakonieczny, A.; Senatorski, J.; Tacikowski, J.; Tymowski, G.; Liliental, W. Computer Controlled Gas Nitriding—A Viable Replacement for Carburising. *Heat Treat. Met.* **1998**, *3*, 46–51.

90. Panfil, D.; Kulka, M.; Wach, P.; Michalski, J.; Przystacki, D. Nanomechanical properties of iron nitrides produced on 42CrMo4 steel by controlled gas nitriding and laser heat treatment. *J. Alloys Compd.* **2017**, *706*, 63–75. [[CrossRef](#)]
91. Michalski, J. *Characteristics and Calculations of Atmospheres for Controlled Gas Nitriding of Steel*; Institute of Precision Mechanics: Warsaw, Poland, 2010.
92. Widi, K.A.; Wardana, W.; Suprpto, W.; Irawan, Y. White layer control on AISI 316L using temperature and gas nitriding diffusion stage process. *Int. Rev. Mech. Eng.* **2017**, *11*, 613–618. [[CrossRef](#)]
93. Yazıcı, M.; Çomaklı, O.; Yetim, T.; Yetim, A.F.; Celik, A. The effect of plasma nitriding temperature on the electrochemical and semiconducting properties of thin passive films formed on 316 L stainless steel implant material in SBF solution. *Surf. Coat. Technol.* **2015**, *261*, 181–188. [[CrossRef](#)]
94. Xi, Y.; Liu, D.; Han, D. Improvement of corrosion and wear resistances of AISI 420 martensitic stainless steel using plasma nitriding at low temperature. *Surf. Coat. Technol.* **2008**, *202*, 2577–2583. [[CrossRef](#)]
95. Takesue, S.; Kikuchi, S.; Misaka, Y.; Morita, T.; Komotori, J. Rapid nitriding mechanism of titanium alloy by gas blow induction heating. *Surf. Coat. Technol.* **2020**, *399*, 126160. [[CrossRef](#)]
96. Abrasonis, G.; Rivière, J.P.; Templier, C.; Muzard, S.; Pranevicius, L. Influence of surface preparation and ion flux on the nitriding efficiency of austenitic stainless steel. *Surf. Coat. Technol.* **2005**, *196*, 279–283. [[CrossRef](#)]
97. Baranowska, J. Importance of surface activation for nitrided layer formation on austenitic stainless steel. *Surf. Eng.* **2010**, *26*, 293–298. [[CrossRef](#)]
98. Priest, J.M.; Baldwin, M.J.; Fewell, M.P. The action of hydrogen in low-pressure rf-plasma nitriding. *Surf. Coat. Technol.* **2001**, *145*, 152–163. [[CrossRef](#)]
99. Lu, S.J.; Zhao, X.B.; Wang, S.K.; Li, J.C.; Wei, W.; Hu, J. Performance enhancement by plasma nitriding at low gas pressure for 304 austenitic stainless steel. *Vacuum* **2017**, *145*, 334–339. [[CrossRef](#)]
100. Wen, K.; Zhang, C.; Gao, Y. Influence of gas pressure on the low-temperature plasma nitriding of surface-nanocrystallized TC4 titanium alloy. *Surf. Coat. Technol.* **2022**, *436*, 128327. [[CrossRef](#)]
101. Avelar-Batista, J.C.; Spain, E.; Housden, J.; Matthews, A.; Fuentes, G.G. Plasma nitriding of Ti6Al4V alloy and AISI M2 steel substrates using DC glow discharges under a triode configuration. *Surf. Coat. Technol.* **2005**, *200*, 1954–1961. [[CrossRef](#)]
102. Wang, B.Y.; Zhou, S.N.; Wang, J.J.; Zhao, B. Effect of Gas Nitriding on CO₂ Corrosion for 35CrMo Steel After Surface Nanocrystallization. *J. Nanosci. Nanotechnol.* **2014**, *14*, 8079–8082. [[CrossRef](#)]
103. Hiraoka, Y.; Watanabe, Y.; Umezawa, O. Effect of Nitriding Temperature and Compositions on Diffusion Layer's Hardness in Gas Nitrided Low Alloy Steel Containing Chromium. *J. Jpn. Inst. Met. Mater.* **2016**, *80*, 253–258. [[CrossRef](#)]
104. Syl, N.; Aliaj, F.; Rama, M. Hardness curves for 31CrMoV9 steel after gas nitriding. *Acta Phys. Pol. A* **2017**, *132*, 484–486. [[CrossRef](#)]
105. Godec, M.; Ruiz-Zepeda, F.; Podgornik, B.; Donik, C.; Kocijan, A.; Balantic, D.A.S.B. The influence of the plasma-nitriding temperature on the microstructure evolution and surface properties of additive-manufactured 18Ni300 maraging steel. *Surf. Coat. Technol.* **2022**, *433*, 128089. [[CrossRef](#)]
106. Michla, J.R.J.; Ravikumar, B.; Prabhu, T.R.; Siengchin, S.; Kumar, M.A.; Rajini, N. Effect of nitriding on mechanical and microstructural properties of Direct Metal Laser Sintered 17-4PH stainless steel. *J. Mater. Res. Technol.* **2022**, *19*, 2810–2821. [[CrossRef](#)]
107. Tong, W.P.; Tao, N.R.; Wang, Z.B.; Lu, J.; Lu, K. Nitriding iron at lower temperatures. *Science* **2003**, *299*, 686–688. [[CrossRef](#)]
108. Lu, K.; Lu, J. Surface nanocrystallization (SNC) of metallic materials-presentation of the concept behind a new approach. *J. Mater. Sci. Technol.* **1999**, *15*, 193–197.
109. Hu, G.; Sheng, G.M.; Han, J. Investigation and Application of Surface Self Nano-crystallization Induced by Severe Plastic Deformation. *Mater. Rep.* **2007**, *21*, 117–121.
110. Azadmanjiri, J.; Berndt, C.C.; Kapoor, A.; Wen, C. Development of surface nano-crystallization in alloys by surface mechanical attrition treatment (SMAT). *Crit. Rev. Solid State Mater. Sci.* **2015**, *40*, 164–181. [[CrossRef](#)]
111. Bahl, S.; Suwas, S.; Ungar, T.; Chatterjee, K. Elucidating microstructural evolution and strengthening mechanisms in nanocrystalline surface induced by surface mechanical attrition treatment of stainless steel. *Acta Mater.* **2017**, *122*, 138–151. [[CrossRef](#)]
112. Ba, D.M.; Ma, S.N. Progress in Researches on Mechanically Induced Surface Self-nanocrystallization Technology of Metallic Materials. *Mater. Rep.* **2006**, *20*, 92–95.
113. Jentzsch, W.D.; Böhmer, S. Investigations on nitride layer formation at the iron surface during gas nitriding. *Krist. Tech.* **1979**, *14*, 617–624. [[CrossRef](#)]
114. Tong, W.P.; He, C.S.; He, J.C.; Zuo, L.; Tao, N.; Wang, Z. Strongly enhanced nitriding kinetics by means of grain refinement. *Appl. Phys. Lett.* **2006**, *89*, 021918. [[CrossRef](#)]
115. Sun, J.; Tong, W.P.; Zhang, H.; Du, X.D.; Wu, Y.C. Enhanced strength and plasticity of gas nitrided iron by surface mechanical attrition pretreatment. *Surf. Coat. Technol.* **2016**, *286*, 279–284. [[CrossRef](#)]
116. Lu, L.; Sui, M.L.; Lu, K. Superplastic extensibility of nanocrystalline copper at room temperature. *Science* **2000**, *287*, 1463–1466. [[CrossRef](#)]
117. Suryanarayana, C. Mechanical alloying and milling. *Prog. Mater. Sci.* **2001**, *46*, 1–184. [[CrossRef](#)]
118. Tao, N.R.; Wang, Z.B.; Tong, W.P.; Sui, M.L.; Lu, J.; Lu, K. An investigation of surface nanocrystallization mechanism in Fe induced by surface mechanical attrition treatment. *Acta Mater.* **2002**, *50*, 4603–4616. [[CrossRef](#)]

119. Sun, J.; Tong, W.P.; Zhang, H.; Zuo, L.; Wang, Z.B. Evaluation of surface-modified 20CrMo by plasma nitriding coupled with ion sputtering and SMAT. *Surf. Coat. Technol.* **2012**, *213*, 247–252. [[CrossRef](#)]
120. Tong, W.P.; Han, Z.; Wang, L.M.; Lu, J.; Lu, K. Low-temperature nitriding of 38CrMoAl steel with a nanostructured surface layer induced by surface mechanical attrition treatment. *Surf. Coat. Technol.* **2008**, *202*, 4957–4963. [[CrossRef](#)]
121. Sun, J.; Tong, W.P.; Zuo, L.; Wang, Z.B. Low-temperature plasma nitriding of titanium layer on Ti/Al clad sheet. *Mater. Des.* **2013**, *47*, 408–415. [[CrossRef](#)]
122. Chemkhi, M.; Reira, D.; Roos, A.; Garnier, C.; Waltz, L.; Demangel, C.; Proust, G. The effect of surface mechanical attrition treatment on low temperature plasma nitriding of an austenitic stainless steel. *Surf. Coat. Technol.* **2013**, *221*, 191–195. [[CrossRef](#)]
123. Balusamy, T.; Narayanan, T.S.N.S.; Ravichandran, K.; Park, I.S.; Lee, M.H. Plasma nitriding of AISI 304 stainless steel: Role of surface mechanical attrition treatment. *Mater. Charact.* **2013**, *85*, 38–47. [[CrossRef](#)]
124. Lin, Y.M.; Lu, J.; Wang, L.P.; Xu, T.; Xue, Q.J. Surface nanocrystallization by surface mechanical attrition treatment and its effect on structure and properties of plasma nitrided AISI 321 stainless steel. *Acta Mater.* **2006**, *54*, 5599–5605. [[CrossRef](#)]
125. Zhang, H.; Qin, H.F.; Ren, Z.C.; Zhao, J.Y.; Hou, X.N.; Doll, G.L.; Dong, Y.L.; Ye, C. Low-temperature nitriding of nanocrystalline Inconel 718 alloy. *Surf. Coat. Technol.* **2017**, *330*, 10–16. [[CrossRef](#)]
126. Liu, D.; Liu, D.X.; Zhang, X.H.; Liu, C.S.; Zhao, W.D.; Xu, X.C. Research Progress in Effect of Surface Deformation Nano-crystalline on Nitriding Behavior of Metallic Materials. *Rare Met. Mater. Eng.* **2019**, *48*, 1352–1360.
127. Sun, J.; Mei, L.Y.; Li, Y.; Lei, Y.Y.; Du, X.D.; Wu, Y.C. Two-Step Nitriding Behavior of Pure Iron with a Nanostructured Surface Layer. *Adv. Eng. Mater.* **2019**, *21*, 1900359. [[CrossRef](#)]
128. Proust, G.; Reira, D.; Chemkhi, M.; Roos, A.; Demangel, C. Electron backscatter diffraction and transmission Kikuchi diffraction analysis of an austenitic stainless steel subjected to surface mechanical attrition treatment and plasma nitriding. *Microsc. Microanal.* **2015**, *21*, 919–926. [[CrossRef](#)]
129. Tong, W.P.; Sun, J.; Zuo, L.; He, J.C.; Lu, J. Study on wear and friction resistance of nanocrystalline Fe nitrided at low temperature. *Wear* **2011**, *271*, 653–657. [[CrossRef](#)]
130. Liu, J.; Ren, Z.; Ma, C. Ultrasonic Nano-Crystal Surface Modification Assisted Gas Nitriding of Ti6Al4V Alloy. In Proceedings of the ASME 2017 12th International Manufacturing Science and Engineering Conference collocated with the JSME/ASME 2017 6th International Conference on Materials and Processing, Los Angeles, CA, USA, 4–8 June 2017.
131. Zhang, C.S.; Wang, Y.; Chen, D.Z.; Wu, Y.Q.; Cui, G.D.; Yang, Y.; Wang, Y.X.; Chen, Y.X. Effect of elemental doping on the catalytic activity of ABO₃ perovskite oxides during low-pressure gas nitriding. *Appl. Surf. Sci.* **2021**, *542*, 148706. [[CrossRef](#)]
132. Aleksandrov, V.A.; Ostaeva, G.Y.; Papisova, A.I.; Papisov, I.M.; Petrova, L.G.; Prikhodko, V.M.; Fatyukhin, D.S. Synthesis of copper-polymer nanocomposite on steel surface and composite-based catalyst for steel nitriding. *Colloid J.* **2015**, *77*, 556–560. [[CrossRef](#)]
133. Kang, K.; Kwon, S.; Lee, C.; Hong, D.; Lee, H.M. Hierarchical analysis of alloying element effects on gas nitriding rate of Fe alloys: A DFT, microkinetic and kMC study. *Acta Mater.* **2019**, *174*, 173–180. [[CrossRef](#)]
134. Nakai, M.; Niinomi, M.; Akahori, T.; Ohtsu, N.; Nishimura, H.; Toda, H.; Fukui, H.; Ogawa, M. Effects of alloying elements on hard ceramic layer formation on surfaces of biomedical Ti-29Nb-13Ta-4.6 Zr and Ti-6Al-4V ELI during gas nitriding. *J. Jpn. Inst. Met.* **2007**, *71*, 415–422. [[CrossRef](#)]
135. Yang, M.; Sisson, R.D. Alloy effects on the gas nitriding process. *J. Mater. Eng. Perform.* **2014**, *23*, 4181–4186. [[CrossRef](#)]
136. Bell, T.; Sun, Y.; Lui, Z.; Yan, M. Rare-earth surface engineering. *Heat Treat. Met.* **2000**, *27*, 1–8.
137. Cleugh, D.; Blawert, C.; Steinbach, J.; Ferkel, H.; Mordike, B.L.; Bell, T. Effects of rare earth additions on nitriding of EN40B by plasma immersion ion implantation. *Surf. Coat. Technol.* **2001**, *142*, 392–396. [[CrossRef](#)]
138. Dossett, J.; Totten, G.E. Fundamentals of nitriding and nitrocarburizing. In *ASM Handbook: Steel Heat Treating Fundamentals and Processes*; ASM International: Materials Park, OH, USA, 2013; p. 619.
139. Podgurski, H.H.; Davis, F.N. Thermochemistry and nature of nitrogen absorption in nitrogenated Fe Ti alloys. *Acta Metall.* **1981**, *29*, 1–9. [[CrossRef](#)]
140. Steiner, T.; Mittemeijer, E.J. Alloying element nitride development in ferritic Fe-based materials upon nitriding: A review. *J. Mater. Eng. Perform.* **2016**, *25*, 2091–2102. [[CrossRef](#)]
141. Meka, S.R.; Jung, K.S.; Bischoff, E.; Mittemeijer, E.J. Unusual precipitation of amorphous silicon nitride upon nitriding Fe-2at.% Si alloy. *Philos. Mag.* **2012**, *92*, 1435–1455. [[CrossRef](#)]
142. Somers, M.A.J.; Lankreijer, R.M.; Mittemeijer, E.J. Excess nitrogen in the ferrite matrix of nitrided binary iron-based alloys. *Philos. Mag. A* **1989**, *59*, 353–378. [[CrossRef](#)]
143. Steiner, T.; Meka, S.R.; Bischoff, E.; Waldenmaier, T.; Mittemeijer, E.J. Nitriding of ternary Fe-Cr-Mo alloys; role of the Cr/Mo-ratio. *Surf. Coat. Technol.* **2016**, *291*, 21–33. [[CrossRef](#)]
144. Steiner, T.; Meka, S.R.; Rheingans, B.; Bischoff, E.; Waldenmaier, T.; Yeli, G.; Martin, T.L.; Bagot, P.A.J.; Moody, M.P.; Mittemeijer, E.J. Continuous and discontinuous precipitation in Fe-1 at.% Cr-1 at.% Mo alloy upon nitriding; crystal structure and composition of ternary nitrides. *Philos. Mag.* **2016**, *96*, 1509–1537. [[CrossRef](#)]
145. Inia, D.K.; Arnoldbik, W.M.; Vredenberg, A.M.; Boerma, D.O. New method for low temperature gaseous nitriding of iron. *Surf. Eng.* **1996**, *12*, 326–330. [[CrossRef](#)]
146. Inia, D.K.; Pröpper, M.H.; Arnoldbik, W.M.; Vredenberg, A.M.; Boerma, D.O. Low-temperature nitriding of iron through a thin nickel layer. *Appl. Phys. Lett.* **1997**, *70*, 1245–1247. [[CrossRef](#)]

147. Mao, C.J.; Wei, K.X.; Liu, X.L.; Yu, X.H.; Hu, J. A novel titanium enhanced plasma nitriding for 42CrMo steel. *Mater. Lett.* **2020**, *262*, 127052. [[CrossRef](#)]
148. Zheng, X.; Zheng, K.; Chang, J.N.; Qu, S.W.; Jia, W.R.; Li, Z.B.; Yu, S.W.; Gao, J.; Ma, Y. Microstructure, mechanical properties and reciprocating wear properties of diamond grits-reinforced NiCrBSi composite coatings on 42CrMo. *Surf. Coat. Technol.* **2022**, *445*, 128703. [[CrossRef](#)]
149. Wei, Y.D.; Liu, Z.R.; Wang, C.Y.; Fan, A.L.; Chen, J.M. A note on coating of surface diffusion-infiltration of Re on steel 20 and armco iron by chemical process. *Acta Metall. Sin.* **1983**, *19*, 121–124.
150. Yan, M.F.; Liu, Z.R.; Zhu, F.Y. Progress in Rare Earth Thermochemical Treatment. *Heat Treat. Met.* **2003**, *28*, 1–6.
151. Jiang, J.H.; Jiang, J.Q.; Ma, A.B.; Zhang, X.H. Application of Rare Earth Addition on the Chemical Heat-treatment. *China Surf. Eng.* **2003**, *16*, 10–14.
152. Hao, S.; Wei, Y.D.; Huang, J.X.; Sun, L. Conducting Materials of PbTiO₃ Ceramics Prepared by Gaseous Penetration of Rare Earth. *Rare Met. Mater. Eng.* **2005**, *34*, 1361–1364.
153. Zhao, W.J.; Liu, G.Q.; Cai, H.; Liu, R.; Chen, C.; Guo, Y.; Wu, Y.P.; Yu, Q.F. Research on Rare Earth Carburized Process of 20Cr2Ni4A Gear Steel. *Foundry* **2018**, *67*, 831–835.
154. Li, S.X.; Gu, M.; Sun, Q.F. Energized function of Ce-rich rare earth content on ion nitriding. *Heat Treat. Met.* **2019**, *44*, 93–96.
155. Pu, S.J.; Yang, H.P.; Wang, H.B.; Wu, X.C. Effect of Rare Earth Ce on High Temperature Friction and Wear Property of Pack Boronized H13 Steel. *Chin. J. Mater. Res.* **2015**, *29*, 481–488.
156. Adijanto, L.; Padmanabhan, V.B.; Holmes, K.J.; Gorte, R.J.; Vohs, J.M. Physical and electrochemical properties of alkaline earth doped, rare earth vanadates. *J. Solid State Chem.* **2012**, *190*, 12–17. [[CrossRef](#)]
157. Cai, X.Y.; Chen, Q.W.; Dai, P.Q.; Yan, Q. Study on Rare Earth Carbonitriding Technology of 20CrMnTi Steel. *Hot Work. Technol.* **2018**, *47*, 233–235.
158. Zhang, G.L.; Xiang, W.M.; Liu, Z.R.; Liu, C.Y. The Rare Earth Boost Infiltrating Technology and the Process. *Heat Treat. Technol. Equip.* **2009**, *30*, 15–21.
159. Wang, B.X.; Zhang, G.L.; Liu, C.Y. Brief Analysis of Rare Earth Nitriding Mechanism. *Heat Treat. Technol. Equip.* **2013**, *34*, 64–69.
160. Li, Q.F.; Li, L.; Liu, E.B.; Liu, D.; Cui, X.F. Temper embrittlement dynamics induced by non-equilibrium segregation of phosphorus in steel 12Cr1MoV. *Scr. Mater.* **2005**, *53*, 309–313. [[CrossRef](#)]
161. Torchane, L. Influence of rare earths on the gas nitriding kinetics of 32CrMoNiV5 steel at low temperature. *Surf. Interfaces* **2021**, *23*, 101016. [[CrossRef](#)]
162. Kielbasa, K.; Arabczyk, W. Studies of the Ammonia Decomposition over a Mixture Of α -Fe (N) And γ' -Fe₄n. *Pol. J. Chem. Technol.* **2013**, *15*, 97–101.
163. Yasuda, N.; Mochizuki, Y.; Tsubouchi, N.; Akiyama, T. Reduction and nitriding behavior of hematite with ammonia. *ISIJ Int.* **2015**, *55*, 736–741. [[CrossRef](#)]
164. Ajikumar, P.K.; Sankaran, A.; Kamruddin, M.; Nithya, R.; Shankar, P.; Dash, S.; Tyagi, A.K.; Raj, B. Morphology and growth aspects of Cr (N) phases on gas nitridation of electroplated chromium on AISI 316 LN stainless steel. *Surf. Coat. Technol.* **2006**, *201*, 102–107. [[CrossRef](#)]
165. Vitry, V.; Kanta, A.F.; Delaunois, F. Application of nitriding to electroless nickel–boron coatings: Chemical and structural effects; mechanical characterization; corrosion resistance. *Mater. Des.* **2012**, *39*, 269–278. [[CrossRef](#)]
166. Peng, T.T.; Dai, M.Y.; Cai, W.; Wei, W.; Wei, K.X.; Hu, J. The enhancement effect of salt bath preoxidation on salt bath nitriding for AISI 1045 steel. *Appl. Surf. Sci.* **2019**, *484*, 610–615. [[CrossRef](#)]
167. Li, J.C.; Sun, F.; Wang, S.K.; Yang, X.M.; Hu, J. Catalysis effect and mechanism of pre-oxidation on direct current plasma nitriding. *Trans. Mater. Heat Treat.* **2014**, *7*, 182–186.
168. Zhen, J.Z.; Shi, Q.W.; Shi, J.; Liu, J.X. Research Progress of Low Temperature Surface Nitriding Technology for Steel Materials. *Hot Work. Technol.* **2019**, *48*, 35–40.
169. Liu, H.; Li, J.C.; Sun, F.; Hu, J. Characterization and effect of pre-oxidation on DC plasma nitriding for AISI4140 steel. *Vacuum* **2014**, *109*, 170–174. [[CrossRef](#)]
170. Güntherschulze, A.; Betz, H. Neue Untersuchungen über die elektrolytische Ventilwirkung: V. Die Eigenschaften der Funken. *Z. Phys.* **1932**, *78*, 196–210. [[CrossRef](#)]
171. Snezhko, L. Anodic Process in Forming of Silicate Coatings.(Translation). *Prot. Met.* **1984**, *20*, 243–245.
172. Zhang, J.T.; Liu, Z.H.; Sun, J.X.; Zhao, H.L.; Shi, Q.Y.; Ma, D.W. Microstructure and mechanical property of electropulsing tempered ultrafine grained 42CrMo steel. *Mater. Sci. Eng.* **2020**, *782*, 139213. [[CrossRef](#)]
173. Rudawska, A.; Jacniacka, E. Analysis for determining surface free energy uncertainty by the Owen–Wendt method. *Int. J. Adhes. Adhes.* **2009**, *29*, 451–457. [[CrossRef](#)]
174. Ma, N. Catalysed gas nitriding process for 30Cr3MoA steel. *Heat Treat. Met.* **2019**, *44*, 150–153.
175. Liu, J.; Liu, Y.J.; Lu, X.F. Investigation on Corrosion Performance of Vacuum Nitriding Layer on 25Cr3Mo. *Foundry Technol.* **2013**, *34*, 695–697.
176. Wang, Z.L. Effect of pre-oxidation on microstructure and properties of the nitrided layer of 40Cr steel prepared by seal pot method. *Heat Treat. Met.* **2019**, *44*, 119–123.
177. Li, J.C.; Yang, X.M.; Wang, S.K.; Wei, K.X.; Hu, J. A rapid DC plasma nitriding technology catalyzed by pre-oxidation for AISI4140 steel. *Mater. Lett.* **2014**, *116*, 199–202. [[CrossRef](#)]

178. Tang, L.; Mao, C.J.; Jia, W.J.; Wei, K.X.; Hu, J. The effect of novel composite pretreatment on performances of plasma nitrided layer. *J. Mater. Res. Technol.* **2020**, *9*, 9531–9536. [\[CrossRef\]](#)
179. Hur, I.C.; Son, K.S.; Yoon, J.H.; Cho, T.Y.; Park, B.G.; Kim, H.S.; Kim, I.S. A study on surface properties and high temperature oxidation behavior of ion nitrided FC-25 gray cast iron. *J. Korean Inst. Met. Mater.* **2005**, *43*, 298–305.
180. Poncet, M.; Issartel, C.; Perrier, S.; Buscail, H. Atmosphere influence on oxidation at high temperature of ni–cr–si model alloys. *Oxid. Met.* **2021**, *96*, 117–127. [\[CrossRef\]](#)
181. Tang, L.; Zhao, X.B.; Li, J.C.; Wei, K.X.; Hu, J. Effect of Pre-Oxidation on Plasma Nitrided Steel AISI4140. *Met. Sci. Heat Treat.* **2020**, *62*, 224–228. [\[CrossRef\]](#)
182. Boynazarov, U.R.; Petrova, L.G.; Brezhnev, A.A.; Bibikov, P.S. Properties of Oxynitride Steel Coatings Obtained Through Three-Stage Processes of Nitriding Combined with Oxidation. *Metallurgist* **2021**, *65*, 886–892. [\[CrossRef\]](#)
183. Lee, S.Y. Mechanical properties of TiN_x/Cr_{1-x}N thin films on plasma nitriding-assisted AISI H13 steel. *Surf. Coat. Technol.* **2005**, *193*, 55–59. [\[CrossRef\]](#)
184. Yilbas, B.S.; Sahin, A.Z.; Ayar, T.; Aleem, B.J.A. Laser nitriding of steel surface: Efficiency analysis. *Int. J. Surf. Sci. Eng.* **2010**, *4*, 492–504. [\[CrossRef\]](#)
185. Yan, G.H.; Lu, S.L.; Zhang, M.L.; Wang, J.C.; Yang, X.D.; Zhang, Z.Y.; Gu, J.F.; Li, C.W. Wear and corrosion behavior of P20 steel surface modified by gas nitriding with laser surface engineering. *Appl. Surf. Sci.* **2020**, *530*, 147306. [\[CrossRef\]](#)
186. Hwang, T.W.; Han, S.W.; Oh, I.Y.; Moon, Y.H. Characterization of the Laser Surface Nitriding of Ti-6Al-4V Alloys in Nitric Acid Solution and Nitrogen Gas Atmosphere. *Korean J. Met. Mater.* **2019**, *57*, 412–421. [\[CrossRef\]](#)
187. Wang, B.; Liu, B.; Zhang, X.D.; Gu, J.F. Enhancing heavy load wear resistance of AISI 4140 steel through the formation of a severely deformed compound-free nitrided surface layer. *Surf. Coat. Technol.* **2018**, *356*, 89–95. [\[CrossRef\]](#)
188. Tinubu, O.O.; Das, S.; Dutt, A.; Mogonye, J.E.; Ageh, V.; Xu, R.; Forsdike, J.; Mishra, R.S.; Scharf, T.W. Friction stir processing of A-286 stainless steel: Microstructural evolution during wear. *Wear* **2016**, *356*, 94–100. [\[CrossRef\]](#)
189. Zong, X.; Wang, H.M.; Li, J.; Cheng, X.; Li, Z.; Tang, H.B. Microstructure characterization and evolution mechanism of titanium during laser surface nitriding. *Mater. Charact.* **2022**, *190*, 112029. [\[CrossRef\]](#)
190. Zhang, M.; Yan, K.; Chen, C.J.; Li, Y.; Wang, X.N.; Hu, Z.R.; Zhang, S.H. Study on TC4 Titanium Alloy used as Valve by Laser Surface Nitriding. *Appl. Laser* **2015**, *35*, 408–414.
191. Wang, C.; Hong, J.; Cui, M.M.; Huang, H.; Zhang, L.; Yan, J.W. The effects of simultaneous laser nitriding and texturing on surface hardness and tribological properties of Ti6Al4V. *Surf. Coat. Technol.* **2022**, *437*, 128358. [\[CrossRef\]](#)
192. Zhecheva, A.; Sha, W.; Malinov, S.; Long, A. Enhancing the microstructure and properties of titanium alloys through nitriding and other surface engineering methods. *Surf. Coat. Technol.* **2005**, *200*, 2192–2207. [\[CrossRef\]](#)
193. Pérez Artieda, M.G.; Fernández Carrasquilla, J. Revisión sobre nitruraciones láser de aleaciones de titanio. *Rev. De Metal.* **2010**, *46*, 530–541. [\[CrossRef\]](#)
194. Zhao, N.Q.; Man, H.C.; Cui, Z.D.; Yang, X.J. Structure and wear properties of laser gas nitrided NiTi surface. *Surf. Coat. Technol.* **2006**, *200*, 4879–4884. [\[CrossRef\]](#)
195. Feng, Z.H.; Sun, X.Y.; Han, P.B.; Fu, H.; Dong, H.C.; Guo, S.; Su, R.; Li, J.H. Microstructure and microhardness of a novel TiZrAlV alloy by laser gas nitriding at different laser powers. *Rare Met.* **2020**, *39*, 270–278. [\[CrossRef\]](#)
196. Kulkarni, A.R.; Manikandan, M.; Shukla, A.K.; Subramaniam, S.; Balaji, V.P.; Palani, I.A.; Jayaprakash, M. Influence of laser-nitriding on mechanical and elevated temperature fretting wear behavior of A356-alloy. *Surf. Coat. Technol.* **2021**, *413*, 127072. [\[CrossRef\]](#)
197. Adachi, S.; Yamaguchi, T.; Ueda, N. Formation and Properties of Nitrocarburizing S-Phase on AISI 316L Stainless Steel-Based WC Composite Layers by Low-Temperature Plasma Nitriding. *Metals* **2021**, *11*, 1538. [\[CrossRef\]](#)
198. Kowalska, J.; Małdziński, L. ZeroFlow-new, environmentally friendly method of controlled gas nitriding used for selected car parts. In *IOP Conference Series: Materials Science and Engineering, Proceedings of the Scientific Conference on Automotive Vehicles and Combustion Engines (KONMOT 2016), Krakow, Poland, 22–23 September 2016*; IOP Publishing: Bristol, UK, 2016; Volume 148, p. 012047.
199. Triki, A.; Gravey, A.; Gravey, P. CAPEX and OPEX saving in SDN-compliant sub-wavelength switching solution. In *Proceedings of the 2015 International Conference on Photonics in Switching (PS), Florence, Italy, 22–25 September 2015*; pp. 262–264.
200. Feng, R.; Lin, P.N.; Hou, C.X.; Jia, S.S. Study of the Effect of China's Emissions Trading Scheme on Promoting Regional Industrial Carbon Emission Reduction. *Front. Resour. Effic. Environ. Impact Assess.* **2023**, *16648714*, 51. [\[CrossRef\]](#)
201. Fu, Y.Z.; Tong, W.P.; Gong, M.Y.; Li, H.Z.; Chen, L.Q. Nitriding of nanocrystalline pure Fe induced by surface mechanical attrition treatment[C]//MATEC Web of Conferences. *EDP Sci.* **2015**, *21*, 08009.
202. Weschenfelder, S.E.; Mello, A.C.C.; Borges, C.P.; Campos, J.C. Oilfield produced water treatment by ceramic membranes: Preliminary process cost estimation. *Desalination* **2015**, *360*, 81–86. [\[CrossRef\]](#)
203. Matera, F.; Listanti, M.; Pióro, M. Recent trends in network planning to decrease the CAPEX/OPEX cost. *Telecommun. Syst.* **2016**, *61*, 205–207. [\[CrossRef\]](#)
204. Baron, P.; Cornet, S.M.; Collins, E.D.; DeAngelis, G.; Cul, G.D.; Fedorov, Y.; Glatz, J.P.; Ignatiev, V.; Inoue, T.; Khaperskaya, A.; et al. A review of separation processes proposed for advanced fuel cycles based on technology readiness level assessments. *Prog. Nucl. Energy* **2019**, *117*, 103091. [\[CrossRef\]](#)
205. Straub, J. In search of technology readiness level (TRL) 10. *Aerosp. Sci. Technol.* **2015**, *46*, 312–320. [\[CrossRef\]](#)

206. Cozzi, L.; Gould, T.; Bouckart, S. *World Energy Outlook 2020*; IEA: Paris, France, 2020; Volume 2050, pp. 1–461.
207. Neumann, J.; Da Rocha, R.C.; Debiagi, P.; Scholtissek, A.; Dammel, F.; Stephan, P.; Hasse, C. Techno-economic assessment of long-distance supply chains of energy carriers: Comparing hydrogen and iron for carbon-free electricity generation. *Appl. Energy Combust. Sci.* **2023**, *14*, 100128. [[CrossRef](#)]
208. Devlin, A.; Kossen, J.; Goldie-Jones, H.; Yang, A.D. Global green hydrogen-based steel opportunities surrounding high quality renewable energy and iron ore deposits. *Nat. Commun.* **2023**, *14*, 2578. [[CrossRef](#)]
209. Wang, H.; Xiao, H.; Zhang, F.J. The Technology Readiness Analysis of Electronic Information System. In Proceedings of the 4th International Conference on Computer, Mechatronics, Control and Electronic Engineering, Hangzhou, China, 28–29 September 2015; Atlantis Press: Dordrecht, The Netherlands, 2015; pp. 845–849.
210. Yaskiv, O.I.; Pohrelyuk, I.M.; Fedirko, V.M.; Lee, D.B.; Tkachuk, O.V. Formation of oxynitrides on titanium alloys by gas diffusion treatment. *Thin. Solid Film.* **2011**, *519*, 6508–6514. [[CrossRef](#)]
211. Yoshida, M.; Ichiki, R.; Utsumi, N. Surface hardening of titanium using gas nitriding. *Int. J. Precis. Eng. Manuf.* **2013**, *14*, 971–976. [[CrossRef](#)]
212. Siyahjani, F.; Atar, E.; Cimenoglu, H. Structural changes on the surface of alloy Ti6Al7Nb under gas nitriding. *Met. Sci. Heat Treat.* **2016**, *58*, 170–174. [[CrossRef](#)]
213. Baranowska, J.; Szczeciński, K.; Wysiecki, M. Increasing of gas nitriding kinetics via surface pre-treatment. *Surf. Coat. Technol.* **2002**, *151*, 534–539. [[CrossRef](#)]
214. Lacaille, V.; Peres, V.; Langlade, C.; Morel, C.; Feulvarch, E.; Bergheau, J.M.; Kermouche, G. Combination of mechanical and chemical pre-treatments to improve nitriding efficiency on pure iron. *Appl. Surf. Sci.* **2017**, *414*, 73–81. [[CrossRef](#)]
215. Díaz-Guillén, J.C.; Naeem, M.; Hdz-García, H.M.; Acevedo-Davila, J.L.; Diaz-Guillen, M.R.; Khan, M.A.; Iqbal, J.; Mtz-Enriquez, A.T. Duplex plasma treatment of AISI D2 tool steel by combining plasma nitriding (with and without white layer) and post-oxidation. *Surf. Coat. Technol.* **2020**, *385*, 125420. [[CrossRef](#)]
216. Wang, Y.; Yin, Y.Y.; Wu, G.L.; Li, L.; Yao, J.H.; Zhang, Q.L. The microstructure and cavitation erosion resistance of Ti6Al4V alloy treated by laser gas nitriding with scanning galvanometer. *Opt. Laser Technol.* **2022**, *153*, 108270. [[CrossRef](#)]

Disclaimer/Publisher's Note: The statements, opinions and data contained in all publications are solely those of the individual author(s) and contributor(s) and not of MDPI and/or the editor(s). MDPI and/or the editor(s) disclaim responsibility for any injury to people or property resulting from any ideas, methods, instructions or products referred to in the content.